Near zero epsilon in Titanium Oxynitride Thin Films: Ab-initio Calculations and Experimental Investigation

ٹائٹینیئم آکسینیٹرائیڈ پتلی فلموں میں صفر ایپسلون کے قریب: ابتدائی قیاس اور تجرباتی تحقیقات

Hafsa Shahbaz

LUMS School of Science and Engineering

Acknowledgments

First and foremost, thanks to ALLAH, the Almighty, for His immense blessing on me throughout my life. Everything i have achieved in my life is due to His thanksgiving.

My gratefulness and regard goes first to my advisor, Muhammad Sabieh Anwar, who provided me with his guidance throughout my research. His enthusiasm for science inspires me constantly to explore new aspects. I could not have imagined having a better advisor and mentor for my MS studies. I also express my warmest and appreciativeness to my co-advisor, Murtaza Saleem, without his keen interest towards research, this work of mine wouldn't be completed in time. He managed from his busy routine to took out time for me and guide me with particularized work. I can't thank him enough for making himself responsible enough for my work and encourage me throughoutly.

Beside the support of my advisor and co-advisor this study could not be completed without the support and kind attitude of my friends, Sauleha Imtiaz, Mahnoor Anjum, Bisma Haq, Wardah Mehmood, Qurat -ul-Ain, who keep me motivated to have patience and tackle the difficulties.

I am overwhelmed to have my great friend, Muhammad Basit, by my side who supported me with his affectionate and helpful attitude. His skills to tackle problem with grace helped me in achieving my tasks within time.

Above all, I am indebted to my family for supporting me throughout my life,

for providing inspiration and for making me what I am today. Specially, the love and care of parents are the deep sources of comfort. My father struggled enough for providing me with best education in order to achieve my goals.

To my Family

Abstract

This study presents the simulation and experimental investigation on electronic and optical properties of Titanium Oxynitride. The computational inspection was performed using full potential-linearized augmented plane wave method (FP-LAPW) based on Density-Functional-Theory (DFT) with the modified Becke-Johnson (MBJ) approximation on WIEN 2k software. From the DFT based simulations, electronic and optical properties such as band structure, density of states, refraction, extinction coefficient, absorption coefficient, epsilon, optical conductivity and reflectivity were extracted.

Furthermore, titanium oxynitride thin films were fabricated using reactive magnetron sputtering. The films were grown using bottom-up approach under varying pressure ratio of oxygen and nitrogen gases working in the background vacuum. Various parameters like; thin films thickness and substrate temperature are changed for achievement of near zero epsilon behavior. Spectroscopy techniques such as x-ray diffraction and scanning electron microscopy were carried out in order to investigate crystallinity, phases and surface morphology of thin films. Spectroscopic Ellipsometry was employed to extract the various optical parameters specifically ENZ response of the thin films. This phenomenon is attributed to the mixture of phases in the thin films. Materials with near zero epsilon behavior is advantageous for designing the enhanced non-linear optical response. The composition dependence of the lattice parameters observed in the grown films is in close agreement with that predicted by the theoretical calculations.

Contents

1 Introduction **12**

1.1 Nano Material and Nano Science 12

1.2 Titanium Dioxide TiO_2 13

1.2.1 Phases of TiO_2 13

1.2.2 Properties of TiO_2 14

1.2.3 Electronic Properties of TiO_2 15

1.2.4 Applications of TiO_2 18

1.2.5 Types of Dopants 19

1.2.5.1 Cationic Dopant 19

1.2.5.2 Anionic Dopant 19

1.2.6 Importance of TiO_2 Thin Films 19

1.3 Titanium Nitride (TiN) 20

1.3.1 Properties of TiN 21

1.3.2 Applications of TiN 22

1.4 Titanium OxyNitride 22

2 Computational Background **25**

2.1 Ab initio Calculations 25

2.2 Many Body problem in Quantum 26

2.2.1 Born-Oppenheimer Approximation 27

2.3 Density-Functional-Theory(DFT) 28
2.3.1 Hohenberg-Kohn Theorems 29
2.3.2 Kohn-Sham Equations 30
2.3.3 Exchange and Correlation Potential 32
2.3.4 Local Density Approximation 32
2.3.5 Generalized Gradient approximation(GGA) 33
2.3.6 The modified Becke-Johnson potential 34
2.4 Full Potential Linearized Augmented Plane Wave method 34
2.5 WIEN2k Code 37
2.5.0.1 Applications of WIEN2k 38

3 Epsilon Near Zero MetaMaterials 41

3.1 Properties of ENZ materials 41
3.2 Optical Constants 42
3.3 ENZ materials 44
3.4 Optical properties of ENZ materials 45
3.4.1 Low Wavenumber 45
3.4.2 Longer Wavelength 46
3.4.3 Group Velocity 47
3.4.4 Protection of Phase 47
3.4.5 Good Absorption 47
3.4.6 Artificial ENZ Metamaterials 48
3.5 ENZ Behavior in Titanium Oxynitride 49

4 Experimental Methods 51

4.1 Simulations 51
4.1.1 Initialization of the calculation 53

4.2 Calculating Properties 54
4.2.1 Electron Density 54
4.2.2 Density of States 54
4.3 Experimental Approach 55
4.4 Sample Preparation 55
4.4.1 Cleaning of the substrate 56
4.4.2 Thin Film Fabrication 56
4.4.3 Deposition by Sputtering 57
4.4.4 Physical Vapor Deposition 58
4.4.5 Chemical Vapor Deposition 58
4.4.6 Magnetron Sputtering 59
4.4.7 RF Sputtering 59
4.4.8 DC Sputtering 59
4.5 Procedure to produce Thin Films 61
4.5.1 Components of instrument 62
4.5.2 Achieving Vacuum in the Chamber 63
4.5.3 Plasma in Chamber 64
4.5.4 Sputtering by DC Power Supply 64
4.6 X-Ray Diffraction (XRD) 65
4.6.1 Scherrer's Equation 66
4.6.2 Working Principle 66
4.6.3 Laue Condition 67
4.6.4 Bragg's Law 68
4.7 Scanning Electron Microscopy(SEM) 68
4.7.1 Components of SEM 69
4.7.1.1 Specimen Chamber 69

4.7.2 Surface Morphology 71
4.7.3 Types of Electron Images 72
4.8 Energy Dispersive X-ray(EDX) 72
4.8.1 Working Mechanism 73
4.8.2 Generation of X-rays 74
4.9 Ellipsometry 75
4.9.1 Working Principle 76
4.10 Raman Spectroscopy 77
4.10.1 Raman Effect 79
4.11 Photoluminescence 80
4.11.1 Components of PL 80

5 Results and Discussion **82**

5.1 Electronic properties 82
5.1.1 Simulations 82
5.1.1.1 Density of States(DOS) 83
5.1.1.1.1 Undoped TiO_2 83
5.1.1.1.2 12.5% N doped TiO_2 84
5.1.1.1.3 25% N doped TiO_2 86
5.1.1.1.4 50% N doped TiO_2 86
5.1.1.1.5 83.5% N doped TiO_2 88
5.1.1.2 Band gap structure of TiO_2 89
5.1.1.3 Optical properties 91
5.1.1.3.1 Real Epsilon(ϵ) 91
5.1.1.3.2 Absorption Coefficient (α) 95
5.1.1.3.3 Reflectivity 96
5.1.1.3.4 Refractive Index 97

5.1.1.3.5 Optical Conductivity (σ) 98
5.1.1.3.6 Extinction Coefficient 99
5.2 Experimental Results 101
5.2.1 XRD 101
5.2.2 SEM 104
5.2.3 EDX 106
5.2.4 Raman Shift 107
5.2.5 Photolumniscence (PL) 108

6 Conclusion **112**

Bibliography **115**

List of Figures

1.1 Three crystallographic phases (a) Anatase, (b) Rutile and (c) Brookite of TiO_2 14

1.2 Schematic of transition of electron from valence band to conduction band. In a) band gap structure of TiO_2, (b) the modified band gap by acceptor type doping in TiO_2, (c) the modified band gap by donor type doping in TiO_2. 17

1.3 Unit cell structure of rutile phase of TiO_2 in two dimensions. . . . 22

3.1 Demonstration of stretching a wave in two different mediums. The wavelength is stretched inside the ENZ medium. In a) Stretching in a ENZ medium. b) Stretching in a medium with ϵ greater than (ϵ_o). 46

4.1 Simulation of TiN_xO_y on Wien2k software. Atoms such that Ti, O and N are selected with their respective atomic number Z and (x, y, z) positions in the lattice. 53

4.2 Various parameters like supercell, muffin tin radius size are chosen according to the required structure of TiO_2 and N doped TiO_2 while performing simulation in wien2k software. 53

4.3 The interface of the simulation after applying the mBJ approximation instead of rnning scf cycle, the files are being saved in the directory. 54

4.4 Schematic of multiple experimental approaches that are being followed in this work. 55

4.5 Demonstration of the working mechanism of the magnetron sputtering. Inside the chamber the plasma is created shown as blue condensed gas with magnetic filed around it. This is formed above the substrate on which deposition is to be done. 61

4.6 Magnetron sputtering unit (DaON 1000S) which is being used to fabricate thin films of TiN_xO_y 62

4.7 System Control unit of the magnetron sputtering instrument. It shows different buttons such as SP targets, O, N and Ar gas flow buttons etc in order to control the functions of the magnetron sputtering machine. 63

4.8 Thin films of TiO_xN_y fabricated by deposition. In a) Thin films of TiO_2 b) Thin films with concentration of 12.5% , 25% ,50% and 83.5% of N doped TiO_2 65

4.9 Schematics of x-ray diffraction and bragg's law. In a) Working principle of x-ray diffraction. b) Representation of bragg's law. . . 67

4.10 Schematic of Scanning-Electron-Microscope (SEM) with all of the basic components which includes condensor lens, electron source, objective lens, detector and a screen to display. 70

4.11 Schematic of Energy Dispersive X-ray (EDX). It is similar to the SEM and records the data with the help of same instruments as that of SEM. 73

4.12 Schematic of the working mechanism of Ellipsometry. It includes linearly polarized light which is incident on the sample and changes it's phase to elliptical polarized light. 76

4.13 Schematic of RAMAN Spectroscopy with it's components laser beam, reflector, transmittor, spectrometer etc. 78

4.14 Rayleigh Scattering, Stokes raman scattering and Anti-Stokes raman scattering between different energy level states in Raman Spectroscopy. 79

5.1 Density of states of TiO_2 a) TDOS and (b-c) PDOS spectra of Ti and O atoms, respectively. 84

5.2 Density of states of TiO_2 and N doped TiO_2(a) TDOS and (b-d) PDOS spectra of Ti, O and N atoms, respectively. 85

5.3 DOS of TiO_2 and 25% N doped TiO_2 (a) TDOS (b-d) PDOS spectra of Ti, O and N atoms, respectively 87

5.4 DOS of TiO_2 and 50% doped TiO_2(a) TDOS and (b-d) PDOS spectra of Ti, O and N atoms, respectively 89

5.5 DOS of TiO_2 and 83.5% N doped TiO_2(a) TDOS and (b-d) PDOS spectra of Ti, O and N atoms, respectively 90

5.6 (a) Band structure of Undoped Ti_O2, (b) refers to 12.5% N doped Ti_O2, (c) refers to 25% N doped Ti_O2, (d) refers to 50% N doped Ti_O2 and (e) refers to 83.5% N doped Ti_O2 92

5.7 Graphs of Real part of epsilon: (a) Simulation of Undoped TiO_2, 12.5% , 25% ,50% and 83.5% N doped TiO_2 (b) Experimental graph of Undoped TiO_2, 12.5% , 25% ,50% and 83.5% N doped TiO_2 93

5.8 Graphs of Absorption Coefficient :(a) Simulation of Undoped TiO_2, 12.5% , 25% ,50% and 83.5% N doped TiO_2 (b) Experimental graph of Undoped TiO_2, 12.5% , 25% ,50% and 83.5% N doped TiO_2 96

5.9 Graphs of Reflectivity :(a) Simulation of Undoped TiO_2, 12.5% , 25% ,50% and 83.5% N doped TiO_2 (b) Experimental graph of Undoped TiO_2, 12.5% , 25% ,50% and 83.5% N doped TiO_2 . . . 97

5.10 Graphs of Refractive index: (a) Simulation of Undoped TiO_2, 12.5% , 25% ,50% and 83.5% N doped TiO_2 (b) Experimental graph of Undoped TiO_2, 12.5% , 25% ,50% and 83.5% N doped TiO_2 98

5.11 Simulation graph of Optical Conductivity of Undoped TiO_2, 12.5% , 25% ,50% and 83.5% N doped TiO_2 99

5.12 Graphs of Extinction Coefficient:(a) Simulation of Undoped TiO_2, 12.5% , 25% ,50% and 83.5% N doped TiO_2 (b) Experimental graph of Undoped TiO_2, 12.5% , 25% ,50% and 83.5% N doped TiO_2 100

5.13 XRD Graphs of (a) Undoped TiO_2, 12.5% N doped TiO_2 , 25% N doped TiO_2, 50% N doped TiO_2 and 83.5% N doped TiO_2 103

5.14 SEM of undoped TiO_2, 12.5% N2 doped, 25% N2 doped ,50% doped N2 and 83.4% doped N2 TiO_2 105

5.15 EdX of undoped TiO_2, 12.5% N2 doped, 25% N2 doped ,50% doped N2 and 83.4% doped N2 TiO_2 106

5.16 Raman Spectra of undoped TiO_2, 12.5% N2 doped, 25% N2 doped ,50% doped N2 and 83.4% doped N2 TiO_2 108

5.17 PL of undoped TiO_2, 12.5% N2 doped, 25% N2 doped ,50% doped N2 and 83.4% doped N2 TiO_2 109

Chapter 1

Introduction

In this emerging scientific world, multiple technologies and inventions are developed to facilitate human life. For advancement of any specific technology or technique, there's a basic ground from which it develops. The accessibility of materials leads to quality and performance of each one of the customary product.

1.1 Nano Material and Nano Science

Nano science is the study of extremely small materials which are visible only through some instruments like electron microscope. This is a vast field which connects different subjects such as physics, chemistry and material sciences together. These nano sized materials have large proportion of surface atoms in a unit volume and their surface energy is almost equal to total energy of the material. In case of nano sized materials, conduction and valence electrons are confined to a small volume and their quantum wavelength is confined to smallest electronic state and is shorter as compare to bulk materials. These quantum confinement effect changes the behavior of the material and precisely impact the various physical properties like electronics and optical response. The thin film technology has

great area of electronic applications, such as solar cells comprised of thin films, Light Emitting Diodes(LED), semiconductor devices such as micro-fabricated devices, IC's (Integrated circuit chips) and many other optical structures. Photo Voltaic devices and solar cells are the most advance devices that are being utilized in this modern technology.

By coating on the substrate called as deposition, layers of thin films are formed and these layers are of order of nano meter or even of smaller dimension which comes in area of miniature devices. The technique of deposition has variety due to existence of different methods available for fabricating materials. Solid, liquid, gas and plasma includes in the states of matter.[1].

1.2 Titanium Dioxide TiO_2

TiO_2 is a "Two Dimensional Nanomaterial (2-D)". These type of nano structured materials have two dimensions outside nanometer range. The thin films, nanosheets, and other 2-D materials (e.g. MOS2 etc.) are examples of 2-D materials. In earth's crust, Titanium is found as the ninth most common element. Titanium dioxide (TiO_2) is the well-known oxide of the titanium metal that occurs naturally in the form of minerals and rocks. TiO_2 is also called as Titania and exists as chemically inert oxide. We are involved in an unfolding story of these fascinating materials and whose main character is Titanium Dioxide (TiO_2). This all started with the photo electrochemical solar energy conversion and then it shifted to the area of environmental photocatalysis.

1.2.1 Phases of TiO_2

Metal oxides belongs to surface science, whose interest is rapidly increasing in relative young field. Titanium dioxide is the most researched surface science in

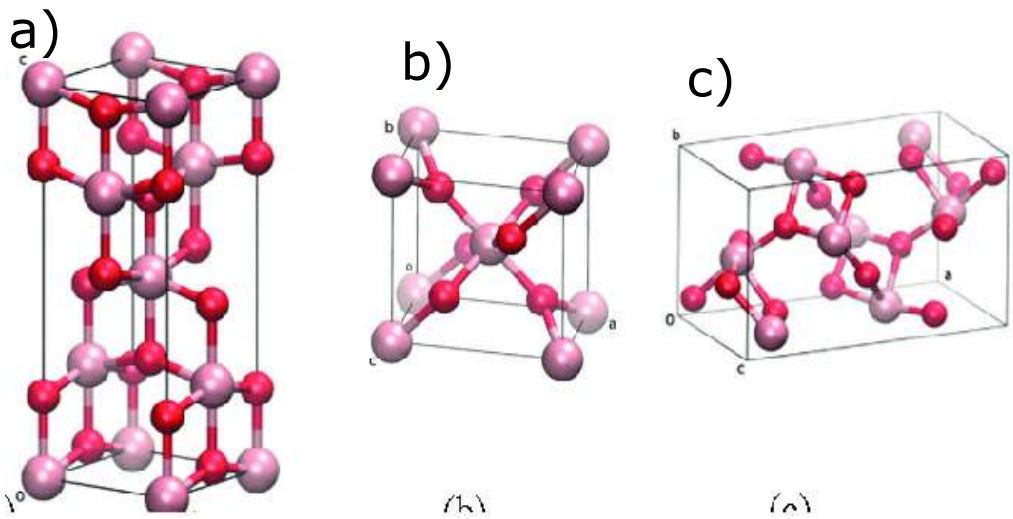

Figure 1.1: Three crystallographic phases (a) Anatase, (b) Rutile and (c) Brookite of TiO_2

the area of metal oxides with it's phases such as rutile and anatase being reviewed thoroughly. Titanium dioxide is decomposed into three crystallographic phases: Brookite, Rutile and Anatase phases as shown in the figure 1.1. Both rutile and anatase phases ensure the tetragonal crystal arrangement whereas brookite comprises the orthorhombic crystal structure. Brookite is a naturally occuring phase and is very difficult to synthesize. Rutile and Anatase are natural occurring but can be synthesized in laboratary. Brookite and anatase are metastable and get converted to rutile phase at higher temperature. These three polymorphs are used for different applications, because the physical properties of every phase is different.

1.2.2 Properties of TiO_2

TiO_2 is well known due to it's easily synthesized and friendly handling properties. It is widely used due to its high electrical and optical properties as well as

Atomic Radius	
O	0.066 (covalent)
Ti	0.146 (metallic)
Ionic Radius	
O^{-2}	0.14
Ti^{+4}	0.064
Crystal Structure	
Rutile	Tetragonal
Anatase	Tetragonal
Brookite	Rhombohedral
Band Gap	
Rutile	3.0(Indirect)
Anatase	3.2 (Indirect)

chemical stability. TiO_2 compound is also considered as thermally stable due its high boiling point (2,972° C) and melting point (1,843° C).

1.2.3 Electronic Properties of TiO_2

TiO_2 is composed of two atoms, which includes Titanium and Oxygen. Titanium atom relates to the Period 4 and Block D while the oxygen atom sites in the Period 2 and Block P of the periodic table. TiO_2 is a solid material with principal ionic character which consists of Ti and O ions:

$$Ti[3d^2 4s^2] \rightarrow Ti^4 + [3d^0(electronicstateofA_r)] \tag{1.1}$$

$$O[2p^4] \rightarrow O^2 - [2p^6(electronicstateofN_e)] \tag{1.2}$$

TiO_2 is a well found semiconductor material with large band gap value (E_g greater than 3 eV). The overlap of the fully occupied oxygen 2p level head towards the formation of valence band (VB), while the 3d orbital overlap of the Ti ions creates the conduction band (CB).

As from the atomic point of view, the following transition corresponding to the intrinsic photo-absorption is observed by TiO_2 solid material:

$$2p(O) \rightarrow 3d(Ti) \tag{1.3}$$

Moreover, doping is the effective way for modifying the electronic property of TiO_2. Doping is complex due to its defective nature. Doping in TiO_2 mainly affects the electronic structure and trap states, which is illustrated by the improvements that are made by doping with elements of equal valences as the host TiO_2 ions. Either substituting the oxygen ($O_2{}^-$) anion or titanium (Ti^{4+}) cation, one can attain doping. Non-metal and metal elements are used for the respective anionic and cationic doping. Such dopants can be substituted in TiO_2 lattice with different techniques i.e sol-gel method, sintering, hydrolysis etc. Band gap may be easily tuned through the better choice of transitional metal-ion doping concentration into TiO_2 which results in shifting in the optical absorption edge towards the visible wavelength range.

TiO_2 is known as an n-type semiconductor owing to the existence of oxygen. According to the reported work anatase band energy has greater value than that of rutile phase. Moreover, the band structure calculation reveals that anatase exhibits indirect band gap, on the other hand rutile has direct band gap. In the case of direct band gap, the minima of valence band and maxima of conduction band takes the similar momentum values but indirect band gap executes different momentum case. In indirect band gap case, electrons are not able to deliver their exact energies and momentum, so for overall conservation, the additional energy quanta i.e. phonon contribution is need to be taken into account.

In the synthesis of TiO_2 thin films, the amorphous or anatase phase is formed generally. There are two basic reasons for anatase phase formation. On the

structural point of view, it would be more ease condition for short ranged TiO_6 octahedral ordering to settle inside the long ranged order of anatase structure due to loosely bonded molecular structure of the anatase than rutile. Whereas, on the thermodynamic point of view, the relatively low surface free energy of anatase phase favours the rapid crystallization. On the other hand, the rutile TiO_2 can be achieved by altering the synthesis conditions e.g. acidity (i.e. PH values) and higher temperature annealing.

TiO_2 phase formation depends particularly upon synthesis parameters or processing conditions. However, the kinetics of such procedures is typically considered in terms of the temperature. For the phase transition of the anatase to rutile, we need a sufficiently high thermal energy to ease the atomic arrangements and to find the minimum energy condition. Structural arrangements and also transformation are occured due to enriched presence of the oxygen vacancy. Under reduced atmospheric conditions, the lower oxygen pressure generally enhances the transformation, while the opposite effect has been detected in vacuum conditions. One commercial form of titanium dioxide is Degussa-P25 with highest surface area.

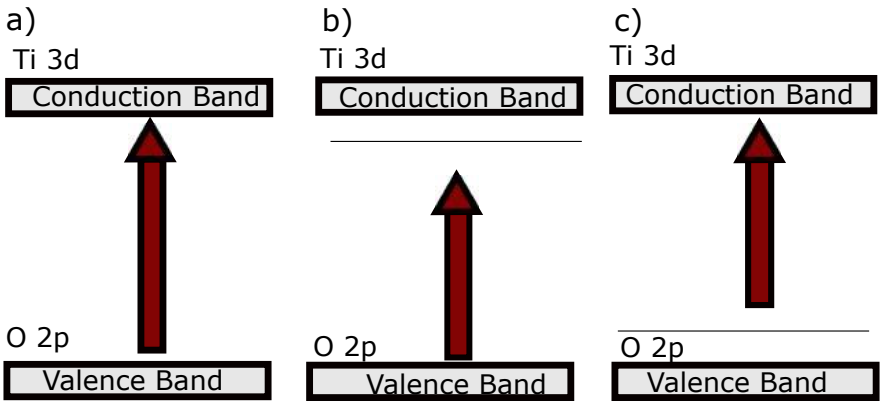

Figure 1.2: Schematic of transition of electron from valence band to conduction band. In a) band gap structure of TiO_2, (b) the modified band gap by acceptor type doping in TiO_2, (c) the modified band gap by donor type doping in TiO_2.

The field of surface science has many discoveries, one of them is unwinding the connection between atomic surface structure and other compound and physical properties. The surface structure is even more stronger on local surface chemistry because of mixed ionic and covalent bonding.

1.2.4 Applications of TiO_2

Titanium dioxide is applied in heterogeneous applications as it acts as a photocatalyst. It find it's uses in solar cells (for the production of hydrogen and electric energy), as corrosive reactive coating, as optical coating and many more[2]. TiO_2 photocatalytic activity due to its strong oxidizing power is considered beneficial for the breaking of the undesirable organic compound inside the water. Moreover, here TiO_2 is also favorable due to its lower cost, extended-time stability and non-toxic chemical nature. Solar cell is the type of device that directly transforms light into electricity. TiO_2 nanomaterials have extraordinary solar energy conversion efficiency. Therefore, they are used in many solar cell applications. These solar cells includes Perovskite, DSSC and QDSC (Quantum dots).
The dopant has a significant effect upon the kinetics of phase transition. Several results have reflected that the dopants have the direct effect in the transformation to rutile. In the particular case, the dopant ions also impact the level of oxygen vacancies by entering to the anatase lattice. Similarly, the lattice constraint may result in the stabilization or destabilization of phase, depending upon the size, content, and valance effects, which results in effecting the transition. Moreover, in case of the dopants or impurities, when the solubility limit exceeds, then their corresponding precipitation can also ease the phase transition through the nucleation

1.2.5 Types of Dopants

1.2.5.1 Cationic Dopant

Several cation dopants have been studied which effect the kinetics of the anatase to rutile transformation. It has been reported that cation having lesser radius and lower valence generally speed up the anatase to rutile transition due to the increased amount of oxygen vacancies produced by cation substitution of Ti ions. On the other hand, when cation having valency greater than 4, it substitutes Ti ions at anatase lattice, which results in the annihilation of oxygen vacancies and also Ti interstitial formation with same or lower valency. Since the charge neutrality generally requires either increased level of the oxygen vacancies or formation of the Ti interstitials having lower valence, so both these doping methods are possible.

1.2.5.2 Anionic Dopant

Anions doping treatment also have keen interest due to it's potential to increase the optical performance of TiO_2 material. There is a very less debate in the literature about the external anions effects to trigger anatase to rutile transition, which is probably due to the improbability that whether the substituent is doped at the desired place or not. It is judicious to accept that anions doping outcomes the filling of the vacancies.

1.2.6 Importance of TiO_2 Thin Films

Due to the unique structure, performance and applications, TiO_2 thin films have become an interesting topic of research in these years.

Researchers have synthesized TiO_2 films by utilizing different raw ingredients in

different methods such as sol-gel, spin coating etc. TiO_2 thin films synthesized with sol-gel method has remarkable characteristics such as it is low cost and have easily controllable parameters. Moreover, heat treatment is an essential parameter for such type of films, because with heat treatment the film crystallinity improves.

It has been reported that TiO_2 thin film also transform from amorphous phase to anatase at certain temperature. The film thickness, grain size and refractive index have also direct relation with the temperature. It has been reported in the result that when temperature rises, the grain size gets larger whereas when film thickness gets reduced, refractive index increases. The presence of metal dopant in the TiO_2 film also plays an important role in varying the chemical as well as physical properties. The optical band gap energy of titanium dioxide nanomaterial has been reported to be shifted in the visible light region for their wide use in solar cell devices.

1.3 Titanium Nitride (TiN)

Titanium Nitride (TiN) belongs to a unique category of materials in which non metallic element "N" of the periodic table forms compound with transition metal Ti. The nature of the bonding is explained by this unusual combination of non metal with a metallic element. Titanium nitride is an interesting material due to it's excellent wear and core resistive properties. Due to it's gold color, it is been used for decorative applications. TiN exhibits superior properties such as excellent temperature durability, chemical stability, corrosion resistance and mechanical hardness. There are different techniques used to characterize these thin films.

Two surface orientations are usually preferred that are <100> and <111>. The

structure of the <100> can be explained by two parameters: plane width (distance between sub planes containing Ti and N atoms) and the distance between average positions of the TiN planes that lies parallel to the surface plane.

1.3.1 Properties of TiN

TiN can be prepared using different methods:

1. Using physical vapor deposition(PVD), Titanium metal powder reacted with nitrogen gas to form a powder compound.

2. Using chemical vapor Deposition (CVD), Titanium Nitride can be formed.

Titanium nitride is considered to be mechanically stable and quenchable. Analysis of the electron density of states and electron localization function reveals that hardness of TiN is strengthened by directional covalent bonds and disappearance of Ti-Ti metallic bonding.
Titanium Nitride is a good selective absorber as it behaves well in high Drude like reflectance and absorption in infrared and visible region. Several researches are done on the crystalline structure of TiN using x-ray and ellipsometric analysis to investigate electronic, optical and transport properties. It is being investigated for plasmonic applications in the range of electromagnetic spectrum. Temperature dependence is one of the prominent aspect of dielectric function in TiN films[3].
Generally, metal ions (e.g. N^{3+}) having lesser number of electrons in valence band comparative to Ti^{4+}, therefore the additional holes forms the acceptor level near TiO_2 valence band. Due to this band gap narrowing, charge transfer occurs at lower energies. However, the visible light photon activity of metal doped TiO_2 is generally due to charge-transfer transition between different bands of O and N.

1.3.2 Applications of TiN

TiN has been a good material in a variety of applications. It is a hard material due to it's high melting point and good conductivity. It stands out due to it's bio-compatibility. In high temperature environments, TiN can serve the purpose of reactive coating sheet. TiN thin films fabricated through lithography have special application in dipolar resonance. It can be replaced with Au nanoparticles due to it's simple spherical shape and no size restrictions and can be easily used in photo thermal therapy. Due to changeable optical properties, TiN is helpful for collecting energy from the sun. It is a promising plasmonic material as it has melting point around 2900° C.

1.4 Titanium OxyNitride

Titanium Oxynitride forms a composite when TiO_2 and TiN gets mixed into eachother. The perfect phase structure form of TiO_xN_y doesn't exist but either TiO_2 or TiN structure can be represented. The unit cell structure of TiO_2 is shown in the figure 1.3

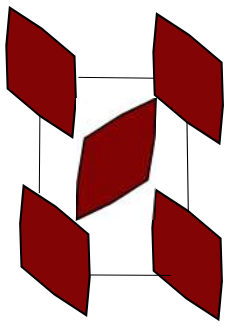

Figure 1.3: Unit cell structure of rutile phase of TiO_2 in two dimensions.

Many studies related to the TiO_2 material have been attempted in order to utilize the dopants for improving various properties. In addition, the overall role

of dopants is included to have the following improvements:

1. TiO_2 optical absorption edge shifting in visible range (reduction in band gap).

2. Enhanced separation of the charge carrier.

3. Introducing the states in the mid of the band gap.

Hence TiO_2 and TiN phases get mixed and improve the overall properties of the thin film.

Chapter 2

Computational Background

These steps in innovation permitted us to use computational method in material science. We can like simulate the chemical responses and see the possible result in technology before the lab's real investigation without bothering about the costly synthetic substances. We have used the method of Density-Functional-Theory (DFT) to explore the electronic and optical findings of TiO_2 and Nitrogen doped TiO_2 in this work.

2.1 Ab initio Calculations

Since the inception of quantum mechanics, ab initio modeling techniques have been around. The rapid increase in the computing power, continuous development of the ab initio techniques makes it popular. There are two possible approaches to use the first principle techniques. The first one make it's direction in discovering interesting properties in novel structures. The other one is to use first principle calculations in combination with experimentally observed phenomena.

2.2 Many Body problem in Quantum

In a system of many particles that are interacting with each other, possibilities are there of multiple interactions of the particles that can be imagined as a whole. The concept of many-body problem is explicitly described. In the event that we assume distinct energy levels of two different atoms, like oxygen and nitrogen, which interact and undergoes different bonding states when brings closer to each other. The characteristics of single atom varies from multiple atoms interacting together.

The systems in condensed matter having multi-electron framework usually related with assemblies large colliding particles. The cores and electrons in atomic configurations are mostly treated with Hamiltonian of large systems for estimation of the total energy and is shown in the Eq. (2.1) [4].

$$\begin{aligned} \hat{H} &= -\frac{\hbar^2}{2m_{el}}\sum_{l}\nabla_l^2 - \sum_{l,L}\frac{Z_L e^2}{\mid r_l - R_l \mid} + \frac{1}{2}\sum_{l\neq m}\frac{e^2}{\mid r_l - r_m \mid} \\ &\quad -\sum_{L}\frac{\hbar^2}{2M_L}\nabla_L^2 + \frac{1}{2}\sum_{L\neq M}\frac{Z_L Z_M e^2}{\mid R_L - R_M \mid} \end{aligned} \tag{2.1}$$

where:

l and m are the subscripts for electrons. L and M are the subscripts for nuclei. And Z_L and Z_M are representing charge and mass of the nuclei, respectively. This coupled problem should be solved principally but this is not possible to solve it due to many body interaction of particles, so an approximation is needed to apply.

2.2.1 Born-Oppenheimer Approximation

Reducing to essential, the first approximation is the **Born-Oppenheimer** approximation. This estimate permits us to neglect one component of the Hamiltonian and that is the active or kinetic energy of the cores as the mass of the nucleus or core is lot bigger than the mass of the electrons and thus electronic and atomic movement can be decoupled. This upgrades calculation process as the count of particles decreases while performing computational work.
This computational data can be expressed in Hartree units: $\hbar = \mathrm{m}_e = 1$. After applying the approximation, Hamiltonian becomes:

$$\hat{H} = \hat{T}_e + \hat{V_{int}} + \hat{V_{ext}} + E_{LM}. \tag{2.2}$$

As shown in the above equation Eq. (2.2), First term is $\hat{T}_{el}$ and which represents kinetic energy of electronic states and is defined in Eq. (2.3) as :

$$\hat{T}_e = -\frac{1}{2}\sum_l \nabla_l^2. \tag{2.3}$$

The second term represents the Coulomb interaction between the electrons as shown in Eq. (2.4)

$$\hat{V_{int}} = \frac{1}{2}\sum_{l\neq m} \frac{e^2}{\mid r_l - r_m \mid}. \tag{2.4}$$

The third term represents electrostatic potential between electrons and nuclei and nuclei is not moving due to it's heavy mass. It is represented in Eq. (2.5) as

$$\hat{V_{ext}} = -\sum_{l,L} \frac{Z_L e^2}{\mid r_l - R_L \mid}. \tag{2.5}$$

Due to the applied approximation, the last term becomes a constant, being independent of electronic wave functions. Thus, we get an Hamiltonian work which includes the coulomb potential and kinetic energy of the nuclei and electrons, as well as various interactions among these.

$$\hat{H}(r_1, r_2, ...r_N)\Psi(x_1, x_2, ...x_N) = E\Psi(x_1, x_2, ...x_N). \tag{2.6}$$

In the event that every one of the argument of our concern are talked about, we can see that in any case the wave function and Hamiltonian of each and every state of electron relies upon 3n-space directions. The system becomes complex when it is difficult to separate the electronic coordinates. We usually deal with problem of single electron system with no other interaction. This will consider as the system of one body if we also exclude the assumption of Pauli's principle which looks manageable. The first electron comes to the lowest state for one electron wavefunction under external potential. Similarly, the connective electrons will go into the respective states and we will never get something like molecules or some other intriguing effects. [5].

Obviously, as a rule, we consider pauli principle to solve a many body problem. According to which, two electrons with equivalent spins can't occupy the same energy state. However, electrons become free in this case and some interesting mechanism relates to interactions cannot be considered.

2.3 Density-Functional-Theory(DFT)

DFT is a well known method to deal with complex many body problems. The charge density is an important element for quantification of many body wave functions in order to solve these complex problems. DFT is most prominent and

widely used technique for estimation of various properties of crystalline materials. The electron density in DFT calculations is considered most important parameter. This makes it more simple to solve the 3-dimensional equations, as now there is only one function "r".

2.3.1 Hohenberg-Kohn Theorems

They proved an inverse relation which states that any observable is exclusively calculated by the density ρ(r). The electronic configuration of ground-state density can be extracted using application of external potential. Kohn and Hohenberg in 1964 stated two theorems and proposed the calculation method for numerical estimation of ground state energy. These two theorems are stated below [6].

1. There is a one to one correspondence between the ground state density $\rho(r)$ of many electron system and unique external potential for a ground state electronic density as shown in Eq. (2.7)

$$< \Psi \mid \hat{O} \mid \Psi >= O[\rho] \tag{2.7}$$

2. If external potential is known, then Energy can be represented in the form of density of electron. By doing minimization, we can predict the ground state density.

They gave the formula that ground state charge density of many interfacing electrons is indistinguishable from that of non-interacting electrons with same elemental charge.

$$\hat{H}_{KS}\phi_i = \epsilon_i\phi_i \tag{2.8}$$

leading to

$$\rho(r) = \sum_{i}^{N} \phi_i^*(r)\phi_i(r) \tag{2.9}$$

where N represents total number of electrons.

From Eq. (2.8) and Eq. (2.9), the KS Hamiltonian is given as

$$E_{HK}[\rho] = T[\rho] + E_{int}[\rho] + \int V_{ext}(r)\rho(r)\, d^3r \tag{2.10}$$

$$E_{HK}[\rho] \equiv F[\rho] + \int V_{ext}(r)\rho(r)\, d^3r \tag{2.11}$$

where:

T[ρ] is the kinetic energy and E_{int} [ρ] is the interaction energy of electrons. Therefore, as in Eq. (2.10) F[ρ] represents combine term of these interaction energies as shown in Eq. (2.11). By combining them, F[ρ] is defined as global function that have association energies that are kinetic and interaction energies being only the function of density. The Hohenberg-Kohn hypothesized the presence of all global functions without estimating the correct mathematical form. E_{HK} reaches it's minimal value for the density of ground state representing V_{ext}.

We have ponder few implications, firstly, there is one to one correspondence between the ground state density and external potential. The quantity density have as much information as the wave function does. Secondly, the contribution of the total energy can be known from these defined quantities of potential. At last, variational principle can be used to find the ground state density

2.3.2 Kohn-Sham Equations

The equations of kohn and sham turned DFT into a practical tool to find ground state density. Density for non-interacting and interacting system was assumed same by kohn and sham. The density of system according to K-S can be formu-

lated as given in following equation as in Eq. (2.12)

$$\rho(r) = \sum_{l} \mid \phi_l(r)^2 \mid \tag{2.12}$$

such that;

ϕ_l is is designated for quasi particle orbitals and can be presented for non-interacting systems [7].

With help of these equations, the ground state energy can be explained as in Eq. (2.13):

$$E_{KS}[\rho] = T[\rho] + E_{xc}[\rho] + E_{Hartree}[\rho] + E_{ext}[\rho] \tag{2.13}$$

where:

T[ρ] is kinetic energy of particles that are independent, $E_{xc}[\rho]$ shows the exchange and correlation potential or energy, $E_{Hartree}[\rho]$ energy appears due to self interaction of charge density, $E_{ext}[\rho]$ is the external energy of the nuclei.

$$\begin{aligned} \hat{H_{KS}} \quad = \quad & -\frac{\hbar^2}{2m_e}\nabla_i^2 + \frac{e^2}{4\pi\epsilon_o}\int \frac{\rho(r\prime)}{\mid r - r\prime \mid} dr' + [V_{ext}[\rho] + V_{xc}[\rho] \\ & -\frac{1}{2}\nabla^2\phi_l(r) + [V_{ext}[\rho] + V_{Hartree}[\rho] + V_{xc}[\rho]]\phi_l(r) \\ & \equiv \epsilon_l\phi_l(r). \end{aligned} \tag{2.14}$$

The kohn-sham orbitals are arrangements of the KS conditions relying upon the charge density. A self reliable arrangement is required, starting from the initial speculation of the electron density and solving KS equations as shown in Eq. (2.14)

2.3.3 Exchange and Correlation Potential

Exchange and Correlation potential $v_{xc}[\rho](r)$ is defined and shown in Eq. (2.15) as:

$$v_{xc}[\rho](r) = \frac{\partial E_{xc}[\rho]}{\partial \rho(r)} \tag{2.15}$$

This term depicts all non trivial many body impacts. The exact equation or form of this quantity is obscure and it must be approximated in any practical utilization of DFT. The accuracy of DFT estimation relies upon the type of guess that is picked.

In the past years, a lot of approximations were put forward and they were arranged in families such as generalized gradient approximation(GGA), meta GGA's and hybrid functionals. John Purdew gave the beautiful idea on how to illustrate these into family. He named these functions as rungs of a ladder that leads to the heaven of chemical accuracy. This is called as Jacob's Ladder of approximations. At the lower part of the ladder lies LDA, that only includes the density and on the second rung lies GGA. And there are multiple approximations available that are described below.

2.3.4 Local Density Approximation

This was the first approximation proposed by kohn and sham while describing their theorems. It explains that the value of E_{xc} energy density at any point in the space or real system is just equal to the energy density of a homogeneous electron gas which have electron density $\rho(r)$ [8]. It is mathematically written in Eq. (2.16):

$$E_{xc}^{LDA} = \int \rho(r) e_{xc}\rho(r)\, d^3r. \tag{2.16}$$

where:

e_{xc} is the XC energy per electron of homogeneous electron gas.

This term e_{xc} which represents energy density is assumed to be constant. Even though this approximation is unique as it was successful in describing total energies and structural properties but this also gives rise to different parametrization such as it predicts wrong electronic band gap.

2.3.5 Generalized Gradient approximation(GGA)

This approximation is widely using for DFT calculations and have so many advantageous over LDA technique. These approximations have strong dependence on the density of local and nearby volumes as the gradient plays a significant role as can be observed from the eq. (2.17). It deals with the gradient of the inhomogeneous systems in contrary to LDA approximation mostly employed to homogenous systems. Further, GGA is considering most prominent for investigation of magnetic structures. But, it somewhat underestimates the evaluation of bandgap determination of semiconducting materials [9].

$$E_{xc}^{LDA} = \int \rho(r) e_{xc}^{G} GA(\rho(r), \nabla\rho(r))\, d^3r. \tag{2.17}$$

In comparison with LDA, GGA tend to improve total energies, atomization energies, energy barriers and structural energy differences. Mathematically GGA can be developed by starting from second order density gradient expansion for the term exchange correlation in the framework of slowly varying density.

2.3.6 The modified Becke-Johnson potential

The modified Becke-Johnson potential by Tran and Blaha (TB-mBJ) was made in form to give correct estimation of the band gap values.
It is modeled after the Becke-Johnson potential as in Eq. (2.18).

$$V_x^{BJ}(r) = V_x^{Slater}(r) + \frac{1}{\pi}\sqrt{\frac{5}{12}}\sqrt{\frac{2\tau(r)}{\rho(r)}}. \tag{2.18}$$

The BJ potential is representing a local potential which minimizes the total energy of the slater determinant of it's corresponding orbitals. The term V_{Slater} was bring forward to formulate the coulomb potential. The TB-mBJ potential is a modification in BJ potential.

$$V_x^{TB-mBJ}(r) = cV_x^{BR}(r) + (3c-2)\frac{1}{\pi}\sqrt{\frac{5}{6}}\sqrt{\frac{\tau(r)}{\rho(r)}}. \tag{2.19}$$

$V_x^{BR}(r)$ is Becke-Rousel exchange potential. While defining calculations of mBJ potential, different parameters are varied to get optimized band gap value. This approximation gives KS band gaps comparable to much more computationally expansive quasi particles band gaps. It is satisfactory for optical calculations.

2.4 Full Potential Linearized Augmented Plane Wave method

This method provides a suitable set of basis of plane waves, the **bloch's theorem** defines that any eigen function $\phi_k(r)$ can be state as the product of some function $\mu_k(r)$ with the periodicity of the lattice, and a plane wave e^{ikr} with $\mathbf{k}$ being any

vector in the region of first Brillouin zone as shown in Eq. (2.20).

$$\phi_k(r) = \mu_k(r)e^{ikr}. \tag{2.20}$$

If there are many plane waves, then they can be sum over all plane waves with the periodicity of the lattice, such that these are the planes waves of corresponding lattice vector **K**.

$$\mu_k(r) = \sum_K c_K^{n,k} e^{iKr}. \tag{2.21}$$

The expression for the $\phi_k(r)$ in plane wave basis set is then repressented in Eq. (2.22)

$$\phi_k^n(r) = \sum_K c_K^{n,k} e^{i(K+k)r}. \tag{2.22}$$

where:

$c_K^{n,k}$ is the coefficient and is need to be determined. The basis set is chosen in a way that it's size must be less than the reciprocal lattice vector K_{max} .

When the regions near the atomic cores are to be described, then by using one of the mixed basis set approach called as Augmented Plane Wave (APW), the space can be divided into two regions. A sphere is drawn around each atom α, which is called as muffin tin sphere, and the space that remains is called as interstitial region I. Electrons near the nuclei behave like free atom and electrons far from it are weakly bounded and well described by plane waves.

One of the APW expression is defined as in Eq. (2.23):

$$\phi_K^k(r, E) = \begin{cases} \frac{1}{\sqrt{V}} e^{i(k+K)r} & r \in I \\ \sum_{l,m} A_{lm}^{\alpha,k+K} \mu_l^\alpha(r\prime, E) Y_m^l(\hat{r\prime}) & r \in S_\alpha \end{cases} \tag{2.23}$$

The position inside sphere is given with reference of the centre of the sphere by $r\prime = r - r_\alpha$. In this length and angles are chosen such that the function in the integral should be similar to the basis set of plane waves with **k+K** at the boundary of the muffin tin sphere. The energy dependence is problematic because in order to describe eigenstate accurately with APW's, E must be equal to eigenvalue, which is not known at this point [10].

In LAPW scheme, adding an additional term to the radial part in order to linearize the energy dependence of radial part such that it no longer depends on the value of the energy E, but on a fixed value E_o.

$$\phi_K^k(r) = \begin{cases} \frac{1}{\sqrt{V}} e^{i(k+K)r} & r \in I \\ \sum_{l,m} (A_{lm}^{\alpha,k+K} \mu_l^\alpha(r\prime, E_o) + B_{lm}^{\alpha,k+K} \mu_l^\alpha(r\prime, E_o) Y_m^l(\hat{r\prime})) & r \in S_\alpha \end{cases} \tag{2.24}$$

Here coefficients in Eq. (2.24) $A_{lm}^{\alpha,k+K}$ and $B_{lm}^{\alpha,k+K}$ are to be determined from the boundary conditions, and it must match the value of the plane wave at the boundary.

If there are multiple states with the same "l" but with different principle quantum number "n", it is optimal to choose not one value of E_o but a set of values of E_o. This can be done by addition of another type of basis set function called local orbital (LO). It is defined as in Eq. (2.25)

$$\phi_{\alpha,LO}^{lm}(r) = \begin{cases} 0 & r \notin S_\alpha \\ \sum_{l,m} (A_{lm}^{\alpha,LO} \mu_l^\alpha(r\prime, E_{1,l}^\alpha) + B_{lm}^{\alpha,LO} \mu_l^\alpha(r\prime, E_{1,l}^\alpha) & \\ + C_{lm}^{\alpha,LO} \mu_l^\alpha(r\prime, E_{2,l}^\alpha) Y_m^l(\hat{r\prime})) & r \in S_\alpha \end{cases} \tag{2.25}$$

where

$E_{1,l}^\alpha$ is set as highest valence state and $E_{2,l}^\alpha$ is set as lowest valence state.

The LO s defined for particular atom α and a particular l and m. These tells us that LO must be normalized and must have a zero value at the muffin tin boundary [11].

Similar thing can be applied to APW method, leading to APW +lo, such as written in form of Eq. (2.26):

$$\phi^{lm}_{\alpha,lo}(r) = \begin{cases} 0 & r \notin S_\alpha \\ \sum_{l,m}(A^{\alpha,lo}_{lm}\mu^{\alpha}_{l}(r\prime, E^{\alpha}_{1,l}) + B^{\alpha,lo}_{lm}\mu^{\alpha}_{l}(r\prime, E^{\alpha}_{1,l})Y^{l}_{m}(\hat{r\prime})) & r \in S_\alpha \end{cases} \tag{2.26}$$

The APW + lo approach has smaller basis size when compared to LAPW approach and not have the problem of energy dependence. This approach is used to describe for valence states such as d and f states with muffin tin smaller in size. DFT was developed to calculate ground state calculations. That's why the excitations of the electrons from ground state to some higher level of state are not well captured. One notable limit of DFT is underestimation of band gap. The band gap issue emerges on the grounds as it is continuous density functional, the necessary dicontinuity jump is absent in it. So, we head towards approximations such as there are approximations available like (mbJ approximation, PBE) which works great to find the band gap of the semiconductor.

2.5 WIEN2k Code

WIEN2k is used as alternative of (APW +lo) basis set inside the atomic sphere to find important parameters of the orbitals. The blend of algorithmic terms of events and increased power had prompted significant improvements in simulations. Now, PC's can be used instead of super computers to make large simulations. This is a full potential and all electron code. The APW +lo method has

made the matrices smaller and so larger data can be studied in less time and with more efficiency.

It should be noted that TiO_2 is a refractory metal. The title of the material, treatment of core electrons, lattice type (cubic, fcc, bcc) and lattice parameters (a, b, c,α, β, γ) are to be chosen. In TiO_2, which is a cubic structure with all angles of 90°C. Desired atoms are to be specified with their atomic number Z, atomic position in the unit cell and size of the muffin tin sphere.

2.5.0.1 Applications of WIEN2k

The calculations done with LAPW method gives the basis for interpreting simulations and comparing it then with the experimental work. The band structure can be compared directly with the experiment in some cases. However, the electronic structure of high correlated systems such as superconductors or transition metal oxides need discussion beyond LDA and GGA.

The calculations done with LAPW method gives the basis for interpreting chemical bonding and comparison with experimental data.

The band structure and relating thickness of states are the most prominent boundaries while deciding the electronic design of a framework. The detailed study of the structure provides information about the electric properties of metals, insulators and semi conductors. By looking into the partial density of states, the interaction between the orbitals or the bonding can be easily determined.

In DFT, electronic density is the key factor. Fourier transform can give static structure quantities which can be compared with experimental data such that by doing XRD under certain conditions of temperature and predicting phases of the crystal structure. In such a case as many parameters are kept constant in order to avoid any systematic error. Size of the atomic sphere, the k-mesh, the

plane wave cut off, the DFT functional etc are some of the parameters need in the computational framework [12]. A modern software package needs a better graphical user interface (GUI). In WIEN2k, this interface is already implemented as w2web.

Chapter 3

Epsilon Near Zero MetaMaterials

Metamaterials are visual structures that can regulate the performance of an electromagnetic wave and exhibit good properties specifically optical properties. The advent of foremost metamaterial was in the medvial era when these were found in artifacts with gold nanoparticles doped in it. The keystone was place by Vesalago by introducing a new name as "negative refractive index" and the introduction to left-hand objects. He said that in order to find these objects, simultaneously relative permittivity and permeability is to be negative. These are called as double ENZ metameterials.

3.1 Properties of ENZ materials

ENZ materials are defined as those materials with value of zero permittivity and are that type of materials which occurs naturally or artificially and reveal exotic behavior at a specific spectral range as ENZ wavelength. Metamaterials which acts as an artificial medium whose permittivity and permeability can be effectively tuned and have the ability to control electromagnetic wave (EM) propagation. Multiple metals like silver, gold and transparent conductive oxides

belong to ENZ materials with their respective wavelengths. Real part of the dielectric constant or permittivity to have zero value is crucial to be called as ENZ material. ENZ metamaterials are hot topic of interest in present studies. They occur naturally and can be fabricated. Theoretical background of these materials depicts properties like phase conservation, static behavior of electromagnetic field and it's capabilities to use in front engineering, subwavelength lensing and super coupling.

3.2 Optical Constants

Optical constant are defined as the basis of latter parts. Epsilon-near-zero objects are introduced and separated. To get an idea of these optical elements, one must have understanding of the basic relations among related quantities. In language of electromagnetism, these relations are defined as [13]:

$$D = \epsilon_o E, \tag{3.1}$$

$$B = \mu_o H. \tag{3.2}$$

where:

D and B represents electric and magnetic flux densities, respectively. E and H represents electric and magnetic fields, respectively. And $\epsilon_o = 8.85 \times 10^{-}12$ F/m is the permittivity and $\mu_o = 4\pi \times 10^{-}7$ H/m is the permeability. The relation of

c and η_o with ϵ_o and μ_o is defined as:

$$c = \frac{1}{\sqrt{\epsilon_o \mu_o}} = 3 \times 10^8 m/s, \tag{3.3}$$

$$\eta_o = \sqrt{\frac{\mu_o}{\epsilon_o}} = 337 ohm. \tag{3.4}$$

Different objects behaves differently with the light intensity within the medium i.e. various substances can have variant features such as isotropicity, homogeneity. Isotropicity is a property that describes the parallelism of an object with respect to a different shape. The value of relative permittivity and permeability is reduced to a scalar value. It is inevitable to accept a tensor count to calculate the permittivity and availability of anisotropic media. The relationship among D and E is defined as shown in Eq. (3.5):

$$\begin{bmatrix} D_x \\ D_y \\ D_z \end{bmatrix} = \begin{bmatrix} \epsilon_{x,x} & \epsilon_{x,y} & \epsilon_{x,z} \\ \epsilon_{y,x} & \epsilon_{y,y} & \epsilon_{y,z} \\ \epsilon_{z,x} & \epsilon_{z,y} & \epsilon_{z,z} \end{bmatrix} \begin{bmatrix} E_x \\ E_y \\ E_z \end{bmatrix} \tag{3.5}$$

where:

D_x, D_y and D_z are the electric flux densities in three planes of axis i.e. x, y and z respectively. Each of these ϵ_{ij} elements are electric tensors and rely upon the material's nature. [14]

The relation between quantities like refractive index (n) and permittivity (ϵ) by applying fourier decomposition on energy functional into exponential form and obtaining refractive index and extinction coeffiecient (κ) as two components of susceptibility χ. From the electromagnetic wave equation, we can get an

expression like in Eq. (3.6)

$$(\frac{kc}{\omega})^2 = 1 + \chi. \tag{3.6}$$

Inside a medium kc/ω have imaginary value and can be written in the form as:

$$\frac{kc}{\omega} = \eta + i\kappa. \tag{3.7}$$

$$\eta = \eta + i\kappa \tag{3.8}$$

The Eq. (3.9) is obtained by solving for real part of these parameters and finding the relation between n, κ and ϵ to get form as in Eq. (3.9)

$$\eta = \sqrt{(\frac{\epsilon\prime}{\epsilon_o}) + i(\frac{\epsilon\prime\prime}{\epsilon_o})} = \sqrt{\epsilon} \tag{3.9}$$

$\epsilon = (\frac{\epsilon\prime}{\epsilon_o}) + i(\frac{\epsilon\prime\prime}{\epsilon_o})$ is defined as permittivity of the medium, also called as dielectric constant.

3.3 ENZ materials

The drude's model determines other metals such as silver with sufficient accuracy. When the frequency "f" of oscillations is higher than ω_p, then the material acts like a dielectric and becomes transparent when lower than ω_p then the material becomes conductive and reflective, acting like a metal [15]. A common practice in the trend of the graph of these epsilon near zero objects is having, around a wavelength of 300nm, value of epsilon goes to zero, termed as epsilon near zero wavelength.

The real part of ϵ transits from positive region (semiconductor state) to negative

region (metallic state) at some specific ranges of wavelength [16], ENZ materials are found in nature and can be also fabricated. The mathematical objects of ENZ comes under the group of zero indexed objects that includes epsilon near zero and mu near zero objects.

There are also ENZ materials, in which, when the value of both of the parts i.e. real and imaginary part of the dielectric constant goes to zero. However, this kind of material is not found in nature and can't be made. Another gate way to achieve the ENZ metamaterials you want to use is multilayer metal dielectric nano-attractive structures because of their simple art.

3.4 Optical properties of ENZ materials

ENZ materials shows particular conduct to standard materials. The qualities of these materials are inter connected and portrayed exclusively. Phase velocity (v_p) of an electromagnetic wave is one in which phase wavefronts moves inside an optical media. The characteristics of electromagnetic wave can be changed either spatially (λ) or temporally (f) by changing the phase velocity while travelling through the medium. It is given in Eq. (3.10)

$$v_p = f\lambda = \sqrt{\frac{\omega}{k}} \tag{3.10}$$

3.4.1 Low Wavenumber

From Eq. (3.11), when the value of ϵ reaches to zero, then the wave vector "k" also goes to zero. The dispersion relation is defined between two quantities i.e.

wave number and frequency and it is written as:

$$k_i = k_o \sqrt{\frac{\epsilon_o \epsilon_m(\omega)}{\epsilon_m(\omega) + \epsilon_o}}. \tag{3.11}$$

where:

k_o is the free space number, ϵ_m is the frequency dependent perimittivity for a conductor.

As described earlier about ENZ wavelength, the dielectric constant of the material varies from metallic to dielectric regime. For really small values of ϵ_m, k_i approaches to zero and the material would require negligible spatial dispersion. The wavefront can be modified by a constant phase shift.

3.4.2 Longer Wavelength

If the permittivity tends to zero as in Eq. (3.10) and Eq. (3.11) then the magnitude of the wavelength is longer at high value of frequency. From this, we can say that electromagnetic wavelength stretches inside the medium as shown in the figure 3.1

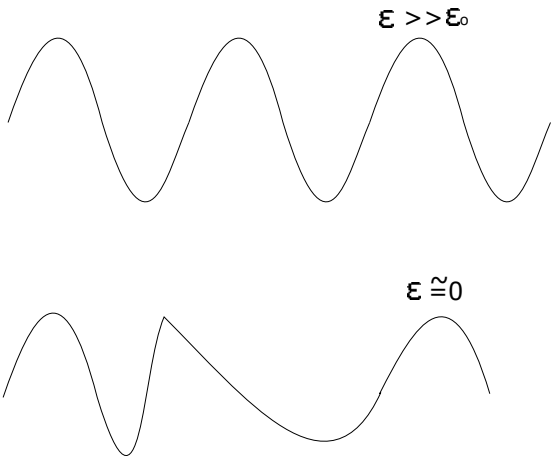

Figure 3.1: Demonstration of stretching a wave in two different mediums. The wavelength is stretched inside the ENZ medium. In a) Stretching in a ENZ medium. b) Stretching in a medium with ϵ greater than (ϵ_o).

3.4.3 Group Velocity

Multiple single waves summed up to form electromagnetic wave. A single velocity is assigned to a group of waves or wave packets and is defined as group velocity (v_g) which can be written as in Eq. (3.12):

$$v_g = \frac{\partial \omega}{\partial k} \tag{3.12}$$

3.4.4 Protection of Phase

The enormous worth of phase velocity inside an ENZ medium prompts to have constraints in wavelength for phase conservation. These changes in a real ENZ system with a small change are not completely preserved [17]. A constant phase has an outcome which assists in changing the wavefront. An E&M entering the ENZ medium with some wavefront will leave with different wavefront. One property of ENZ material is to emit the light at subwavelength range after striking from it. At the same time, the medium will isolate distances between focuses (amplifying resolution) to make it readable by magnifying the images.

3.4.5 Good Absorption

Wonderful absorption has crucial and mechanical applications. The total absorption can be used in practical usage for good proficiency of energy change. In conductive oxides, specifically TCOs (Transparent Conductive Oxides), the epsilon is regulate by varying concentration of impurities added. In view of the doping thickness, ENZ frequency can be characterized in a specific unearthly area supposed as the ENZ region. Because of the change from dielectric to the metallic state in the ENZ frequency, the subwavelength of TCO films can introduce

plasmonic properties [18].

3.4.6 Artificial ENZ Metamaterials

Using a proper composition of metallic and dielectric materials, one can design a subwavelength structure with ENZ behavior in the visible range. Such structures are known as hyperbolic metamaterials (HMMs), which exhibit effective permittivities with different signs in the parallel and perpendicular orientation of the crystal. Among these materials, nitrogen doped TiO_2 has shown particular promise, because of it's potential for low cost fabrication. In addition annealed TiN_xO_y have faster recombination time than many semiconductors.

The permittivity of TiN_xO_y can be described by drude model, where the incident light interacts with the free carriers in the material, and their response becomes resonant at the plasma frequency. Based on this model, the real part of the permittivity crossed zero at the frequency "ω_o" which is given by in Eq. (3.13):

$$\omega_o^2 = [\frac{q^2}{\epsilon_o \epsilon_\infty m^*}]N - \frac{1}{\tau} \tag{3.13}$$

where:

q is the elementary charge, ϵ_o is vacuum permittivity, ϵ_∞ is permittivity at higher frequencies.

By utilizing an arranged pattern of metallic and dielectric materials, one can plan a subwavelength structure with ENZ conduct in the noticeable reach.

However, it remains an open question that how to best process an ITO film in order to control each parameter i.e. how the plasma frequency is precisely controlled and achieve uniformity. In all previously reported ENZ TiN_xO_y thin films, the thickness of these films were significantly less than the wavelength, that

can fully benefit from the ENZ property.

3.5 ENZ Behavior in Titanium Oxynitride

There are alot of intermediate phases present for general composition of TiNxOy called as Titanium Oxynitride. This is found in midway of TiN and TiO_2. The properties are similar to those of the respective parent materials such that the composition is same that of the pure system. When they evolve from one phase to another, there is a change in properties. Preparation of Titanium Oxynitride through either oxidation of TiN or Nitridation of TiO_2 is not straightforward. On one hand, the oxidation of the TiN quickly leads to the formation of TiO_2 and on the other hand, nitrogen implantation in TiO_2 leads to substantial reconstruction of the surface due to strong reduction.

Chapter 4

Experimental Methods

4.1 Simulations

Computational details of TiN_xO_y are found out by performing simulations. By using WIEN2k software to perform this task with GUI interface, desired data is obtained. We can have structural and optical properties from the data. This work focuses on Undoped TiO_2 and then different concentration of nitrogen is being doped into TiO_2 to see the effect of this doping. Various parameters like electron density, band structure, refractive index, Density of States are found out. This simulation is done by following the below described steps:

1. Give Title to the calculation as Titanium oxynitride or TiN_xO_y and select relativistic treatment for the core states.

2. Select the desired atoms such as Ti, O and N for forming titanium dioxide and titanium oxynitride structure. Their atomic number "Z" is generated automatically.

3. Select their respective space group and lattice parameters either in $\AA$ or a.u units.

PARAMETERS	
Title	TiO_2 AND $TiN_{2-x}O_x$
Lattice	Tetragonal
a	4.594
b	4.594
c	2.958
α, β, γ	90°
Atom	Ti enter position (0,0,0)
Atom	O enter position (0,0,0)
Atom	N enter position (0,0,0)

4. Then, select the structure type as cubic, in my case, with all angles and lattice parameters being equal. The number of points in radial mesh are selected and first radial mesh are set to default values.

5. Muffin tin radius should be chosen such that it must be large enough but not be overlapping. In my approximation technique for forming structure, radius size is set to default value.

6. Then, the atomic position must be specified and only for one equivalent atom Ti, other symmetrical atoms are automatically generated as defined by the space group. Do this procedure for second atom O and then third atom N as shown in figure 4.1. This will generate a file for a structure.

Figure 4.1: Simulation of TiN_xO_y on Wien2k software. Atoms such that Ti, O and N are selected with their respective atomic number Z and (x, y, z) positions in the lattice.

4.1.1 Initialization of the calculation

After selecting all the required parameters, execute the initialize calculation tab on the task menu and a screen will pop up. Choose quantities as per required such as xnn, x sgroup , x symmetry, instgen lapw , x lstart and x kgen etc as represented in figure 4.2. This will create files in the directory that we have saved. Apply "mBJ approximation" instead of clicking on tab run scf cycle. This

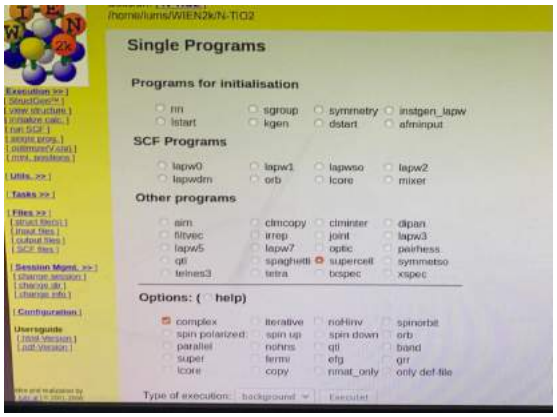

Figure 4.2: Various parameters like supercell, muffin tin radius size are chosen according to the required structure of TiO_2 and N doped TiO_2 while performing simulation in wien2k software.

approximation is set of codes and do the same task as this scf cycle does. It runs the files in the background to load data as shown in figure 4.3

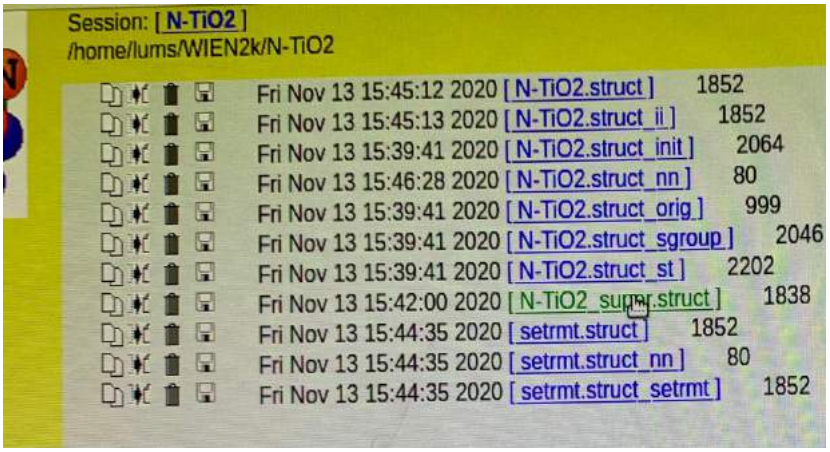

Figure 4.3: The interface of the simulation after applying the mBJ approximation instead of rnning scf cycle, the files are being saved in the directory.

4.2 Calculating Properties

4.2.1 Electron Density

Select El. Dens from the task menu and run it. Click on the buttons one by one and keep in mind to not to click the button twice on a specific tab. There will be option to get the plot of it. It is shown in result section 5.

4.2.2 Density of States

Similarly, follow the same procedure of selecting Density of states from the task menu and run it. In the same way all the other desired parameters such as Reflectivity, Extinction Coefficient etc are found out and the obtained graphs are attached in the Result and Discussion section 5.

4.3 Experimental Approach

The whole experimental course involved during and after the samples synthesis can be summarized in the block diagram arrangement. Their structural analysis and phase purity were determined using x-ray diffraction (XRD) technique. For study of the rotational, vibrational and the other low-frequency modes, Raman spectroscopy was performed and surface topography was done using the Scanning electron microscopy (SEM).

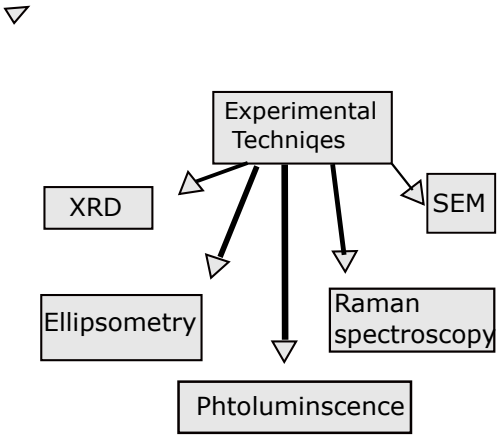

Figure 4.4: Schematic of multiple experimental approaches that are being followed in this work.

4.4 Sample Preparation

Sample preparation is precisely the first step in the experimental processing. Various procedures can be engaged for the synthesis of samples. For synthesis of samples, the main experimental tools involved to prepare the precursor solution and deposition of titanium oxides film are explained in this section.

4.4.1 Cleaning of the substrate

There's a proper method that is being followed for substrate cleaning. This is little but important step as desired results depends on the factor that how much cleaned a substrate is. I have followed below steps:

1. Wear gloves in order to ensure that our hands are protected from these chemicals and our substrate has no contact with fingerprints of our hands.
2. Take a <100> silicon substrate and place it's shiny side on a clean wipe.
3. Clean the substrate first with the help of soap and rub it softly.
4. Fill a beaker with deionized water and by using tweezer put the substrate in the beaker. Put this beaker into the sonicater and let it run for 3 minutes.
5. Fill another beaker with acetone and put substrate inside it and run sonicator for atleast 4 minutes.
6. Add isopropyl alcohol(IPA) and run sonicator again for 2 minutes and at the end again put the substrate inside the DI water.
7. Let the water vapours on the sample dry from a pressure gas and the substrate is cleaned then.

4.4.2 Thin Film Fabrication

In order to produce Titanium oxynitride thin films for ENZ behavior, the fabrication of these films with required structural phases is very important. This is now not a difficult task as the modern deposition techniques are into field, such as atomic layer deposition, DC and RF magnetron sputtering which allows very precise control on the parameters for obtaining required phases. The true

challange lies in forming TiN_xO_y films of desired phases while maintaining ENZ behavior.

An efficient method to produce charge carriers is to induce oxygen vacancies in the TiN_xO_y films, which can be achieved by annealing in vacuum which causes outward diffusion of oxygen. As the valency of oxygen is 2, each o-vacancy contributes two electrons for conduction. Thus a fine balance is necessary in order to achieve films of good quality. In short, content of oxygen in deposition is important. If less amount of oxygen is deposited then it behaves somewhat like metal and if great amount of oxygen is deposited then it behaves more of like semiconductor. Further, composite phases of TiO_2, TiN and TiN_xO_y plays vital role in ENZ behavior for fabrication of Titanium oxynitride thin films.

4.4.3 Deposition by Sputtering

Among above portrayed strategies, sputtering assumes a significant part in actual properties of the nanoparticles of various materials and also for thin films. Sputtering is standout amongst other deposition techniques. In this cycle, substrate is utilized on which target material is to be deposit. The environment is completely vacuum cleaned to such an extent that all the contamination is filtered out. The target is sputtered towards substrate through sputtering guns. Turbo molecular pump is used to make high required vacuum for thin film fabrication. RF and DC are principle kind of sputtering process in creating testimony deposition innovation.

Morphology and crystallinity of thin films play a vital role for obtaining required properties of a material. In order to produce thin films, certain parameters should be keep in mind. With the varying deposition conditions to form thin films, the mechanical, electrical, optical and morphological parameters changes. The re-

sponsive gas stream and partial pressure, working pressure and deposition temperature are significant parameters.

By utilizing sputtering technique, single layer of semiconductor compound along with different thickness of core layers are outlined. Deposition process might be repetitive for numerous times while making metal and insulator films. The deposition process is partitioned into two fundamental classes i.e. Chemical and Physical Vapor Deposition.

4.4.4 Physical Vapor Deposition

During PVD, the target or the source material is put in an surrounding full of ionized or energetic atoms and electrons are escape from target surface and consolidate on the substrate surface. Sputtering, Molecular Beam Epitaxy, Pulsed Laser Deposition (PLD) are fundamental sort of PVD methods. In these techniques, thermodynamical or mechanical cycles are followed to produce TiO_xN_y.

4.4.5 Chemical Vapor Deposition

Atomic deposition is one of the normal kind of chemical vapor deposition. In this technique, chemical deposition are utilized to create thin films. By presenting the substrate to volatile originators to respond or rot on substrate. Few of the advantages of sputtering deposition in present day film technology are:

1. High deposition (via magnetron sputtering).

2. Great quality authority over the film synthesis and microstructure.

3. Adaptability to deposit combinations and mixtures of different kinds and diverse fume pressure.

4. Using a gas in the chamber as a medium to react to deposit compounds from essential targets.

In this work, we fabricate TiO_2 and Nitrogen doped TiO_2 thin films.

4.4.6 Magnetron Sputtering

In magnetron sputtering method, a magnet produce a strong magnetic field which at that point center the plasma by capturing the electron. The fundamental guideline of magnetron sputtering is basically to do the sputtering of thin films and, in this process, the sample is being excited by some high energetic ions of Argon (Ar) gas. In this process, the plasma remains close to the guns to protect the other components from any mishap. Magnetron sputtering is one of the best techniques for the fabrication of thin films. The sputtering unit we've in our research lab has two kinds of power supplies which are: DC and RF power supply. But, in general, we can also make use of both power supplies at once making arrangements in system. [19]

4.4.7 RF Sputtering

On account of RF magnetron sputtering system, the electrons are generated for longer distance, enabling it to generate stable and high density plasma. It uses non-conductive target material for deposition. Due to use of a magnet, it might have more effort in making thin film.

4.4.8 DC Sputtering

The DC sputtering is utilized due to some of drawback of elementary technique of RF sputtering set-up. This is simple superficially and in this electrically neutral Argon ions are accessible into a vacuum chamber at a pressuring factor of (1 to

10) mTorr. The plasma is produced by applying a high DC voltage between the substrate and the sample (target), which then ionize the Ar gas. The Ar gas situated in the chamber is extremely hot and the plasma produced, in this way, glows inside the discharge tube because of that it's called "Glow discharge Tube Plasma".

Argon ion sputtering is a Physical Vapour Deposition (PVD) method for producing thin films of a material. This actually works on the mechanism of running current through an inert gas, usually argon, under high vacuum to ionize the Ar gas forming plasma of Ar^+ and electrons. A constant negative voltage is supplied, which ionizes argon atoms and afterwards producing plasma. Magnetic field is produced by magnets that is mounted behind the target, which expands the ionization pace of the Argon gas. The ionized Argon ions are then accelerated by the electric field and head towards the negatively charged cathode where they strike and sputter atoms from the target. Magnets are placed under the target anode in order to trap electrons such that to not to bombard the substrate and allow for faster deposition rates. These atoms then travel through the plasma in the form of vapour and then condense on the surface of the substrate forming thin films. We can also rotate the substrate stage to achieve even more improved deposition.

In DC magnetron sputtering, the negative voltage is applied by the cathode placed at the top. At the cathode, target (titania) is placed and from there it can be deposited on the substrate to form thin film.

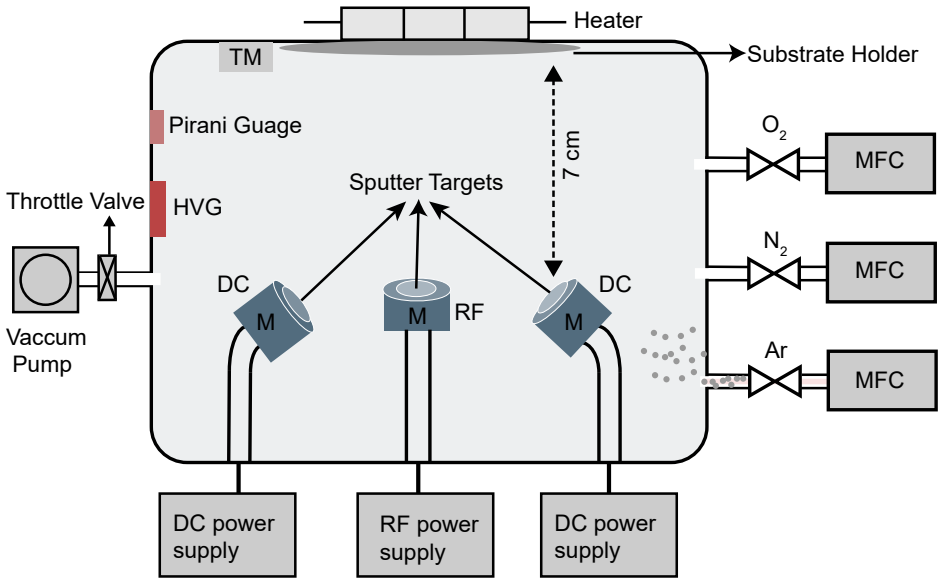

Figure 4.5: Demonstration of the working mechanism of the magnetron sputtering. Inside the chamber the plasma is created shown as blue condensed gas with magnetic filed around it. This is formed above the substrate on which deposition is to be done.

The target goes about as an anode in DC mode or is conductive. On the off chance that the target is insulator, positive argon ions coming from the plasma would be striking negatively charged target, causing collection of charge at the target surface, that would diminish the negative surface voltage, afterward there will be no plasma.

4.5 Procedure to produce Thin Films

In my experiment, DC sputtering method is applied to deposit Titanium Oxynitride. In this case, nitrogen and oxygen acts as reactive gases that are being introduced into the chamber of sputtering unit along with Argon plasma. During the deposition process, N_2 and O_2 will decomposed into atomic nitrogen and oxygen, which combines with the sputtered titanium atoms. This reaction will occur on the surface of the wafer. i.e that surface of the target itself. Silicon wafer

was the substrate. Magnetron sputtering unit (DaON 1000S) was the instrument used for depositing thin filmsa as shown in the figure 4.6.

Figure 4.6: Magnetron sputtering unit (DaON 1000S) which is being used to fabricate thin films of TiN_xO_y

4.5.1 Components of instrument

There are two major components: components which are outside the main body and the components which are inside the body. Components which are outside the main body includes: a transformer, a chiller and a compressor which compresses the gas. And inside components of main body includes: a chamber in which vacuum is generated, three guns (one is an RF and two DC guns), an ultrahigh voltage pump, a turbo molecular pump, a high vacuum gauge, two power lines (one DC and one DC) and a temperature controller.

1. At First, turn on the chiller, compressor and transformer.

2. After that switch the main power ON by inserting a key and pressing Reset Green button.

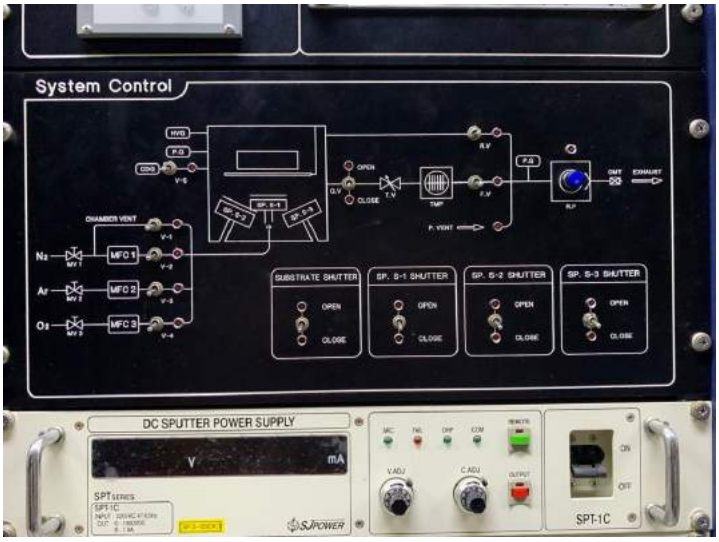

Figure 4.7: System Control unit of the magnetron sputtering instrument. It shows different buttons such as SP targets, O, N and Ar gas flow buttons etc in order to control the functions of the magnetron sputtering machine.

3. The working procedure inside the chamber is to close all the valves other than the vent valve of the chamber. And the substrate is mounted on the shutter which is right above the chamber.

4. After that target shutters were opened where Titania was placed and the guns were placed with 5.0cm apart from substrate holder as shown in the figure 4.7

5. The RP (Rotary Pump) was turn ON after pushing the chamber door.

4.5.2 Achieving Vacuum in the Chamber

Vacuum of 5×10^{-6} Torr was achieved by opening all the valves expect RV. After achieving the required vacuum value, RV (rotatoty valve) was closed but Rotatory pump was still ON.

Parameters	
Initial Pressure	$5\times10^{-}6$
Working Pressure	0.005 Torr
Voltage	400V
Deposition Time	2 or more hours
Rotation	yes

By high vacuum gauge, the vacuum pressure 5×10^{-6} Torr was accomplished in 30 to 40 minutes.

4.5.3 Plasma in Chamber

First and foremost, the substrate was set to 300∘C by using temperature regulator. The rotation of substrate holder was set as 10 rpm. The Argon gas valves were opened and it begins to flow after pressing button on MFC controller.

4.5.4 Sputtering by DC Power Supply

DC power supply was turned ON after opening the shutter SP2. Pressure was dropped automatically to working pressure after changing TVC button to open condition and it was kept at 20 mTorr. Plasma was generated then and substrate shutter was opened in order to sputter the target for atleast 30 minutes.
The temperature was set to zero after deposition. The rotation, MFC and Ar gas was also stopped. Every component such that Target shutter, Force valve, Rotatory pump, chamber vent were closed and target and substrate were un-mount. After few hours when the temperature of substrate comes to room temperature then the thin films were collected. Thin films are shown in the figure 4.8

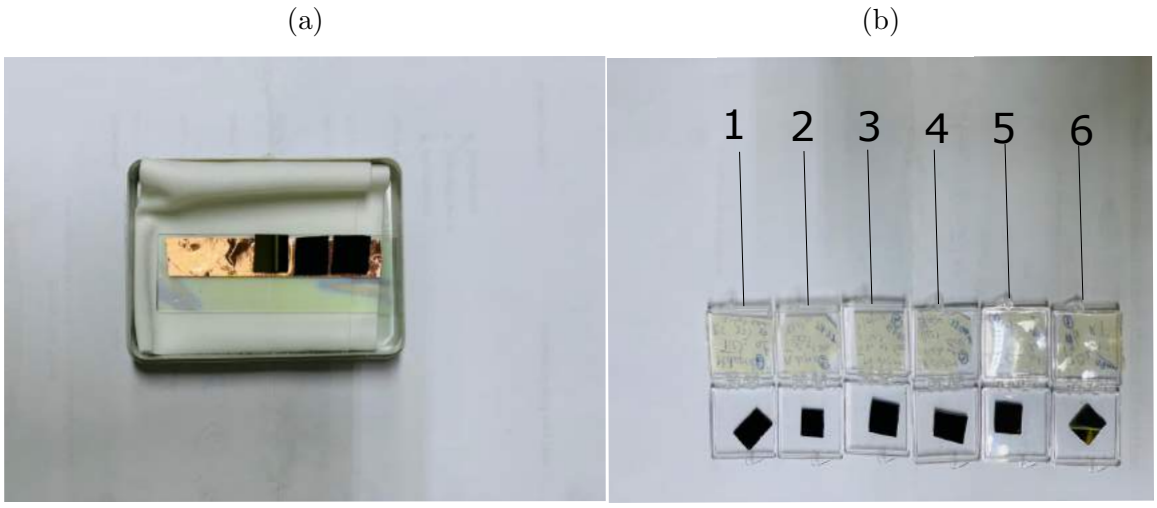

Figure 4.8: Thin films of TiO_xN_y fabricated by deposition. In a) Thin films of TiO_2 b) Thin films with concentration of 12.5% , 25% ,50% and 83.5% of N doped TiO_2

4.6 X-Ray Diffraction (XRD)

XRD is a non damaging strategy used to portray crystalline materials and to determine the atomic construction of the crystal. Usually, the wavelength used is about 0.1-10 A^o. This makes it conceivable to extract data from interatomic distances, bond angles, phase orientation and identification and crystallite sizes. A unit cell is defined as several atoms placed in a fixed arrangement. When these unit cells are placed in a lattice, they form a crystal. A crystal composed of planes of atoms that are positioned at distance 'd' from each other in a crystal structure. A trademark XRD pattern is created by plotting identified x-ray intensities as a function of angle '2θ'. The peak intensities at various diffracted angles are used to discover the crystallographic directions of the necessary sample. The intensity tells about the complete region under the peak as shown in the figure 4.9

TiN_xO_y films fabricated exhibits growth along a few Miller index directions, as well as an extra phase. If the size of the peaks is smaller then it is showing

crystallites embedded in amorphous matrix. Moreover, films fabricated at lower temperatures are amorphous in their phase. If the temperature at which the deposition process occurs is higher, then crystallinity would be better. Crystallographic analysis of thin films was performed using XRD for observation of crystallinity and plane orientations.

4.6.1 Scherrer's Equation

We can find the crystal size using the "Scherrer Equation":

$$D = \frac{K\lambda}{\beta \cos\theta} \tag{4.1}$$

where:
D is the crystallite size of the particle, K is Debye Schrrer constant (K=0.94), λ is wavelength of CuKα radiation (0.154nm), β is Full Width Half Maximum(FWHM) and θ is bragg's angle. Debye Schrrer formula gives information about the lower bound of the particles and give little information about the strain.

4.6.2 Working Principle

The idea that crystals could be used as a diffraction grating for X-Ray arose in 1912. XRD crystallography is an ubiquitous idea utilized for finding crystal structure. Atoms arranged in a regular pattern form electron density planes so that the incoming radiation can scatter from the planes. The x-ray wavelength is about as the magnitude of crystallographic spacing i.e 0.1-10 A^o.

Samples are mounted on goniometer with multiple angles of freedom where the detector or X-ray source can be moved easily. This produces a series of X-ray

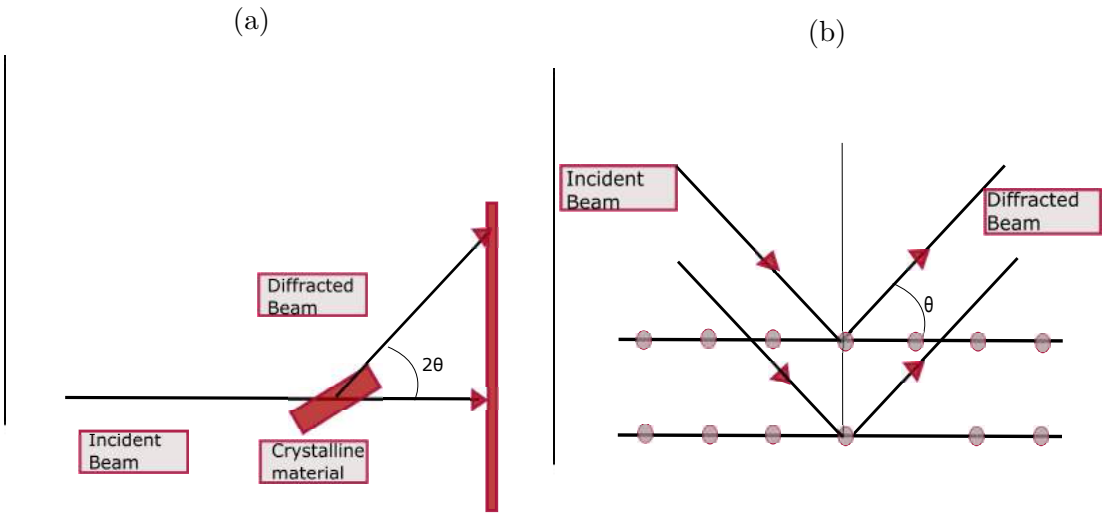

Figure 4.9: Schematics of x-ray diffraction and bragg's law. In a) Working principle of x-ray diffraction. b) Representation of bragg's law.

count peaks (Bragg Diffraction peaks) in y-axis as function of angles (θ) on x-axis as shown in the figure **??**. We have used CuKα radiation (1.514 A) at an angle of 0.75° [20].

4.6.3 Laue Condition

In a crystalline solid because the atoms are arranged in a regular three dimensional lattice/arrays, constructive interference of the scattered X-rays will take place. This can be described mathematically by von Laue diffraction

$$\begin{aligned} a(cos\gamma 1 - cos\sigma 2) &= h\lambda \\ b(cos\gamma 2 - cos\sigma 1) &= k\lambda \\ c(cos\gamma 3 - cos\sigma 3) &= I\lambda. \end{aligned} \tag{4.2}$$

where:

a,b and c are lattice spacing. σ is incident X-ray beam, γ is diffracted X-ray

beam and I are natural numbers [21].

4.6.4 Bragg's Law

The implementation of Laue condition is difficult to tackle due to consideration of parameters in large amount. Bragg offered a more physical model in which diffraction peaks occurs if the length of photon's path between any two scattering centers in a unit cell is integar multiple of the photon wavelength. Such that it is scattered as a spherical waves which can then interfere constructively or destructively. Such that d(hkl) is the distance between the atomic planes in a crystalline solid, defined by the hkl-Miller indices, θ is angle between the incident X-ray beam and crystal lattice planes and λ is the X-ray wavelength, so scattering is define by the analogy of diffraction from a grating by the relation:

$$2dsin\theta = n\lambda \tag{4.3}$$

where

n is the order of diffraction, d is the distance between the atomic planes in a crystalline solid and λ is the X-ray's wavelength.

4.7 Scanning Electron Microscopy(SEM)

SEM is a device which allows us to observe, investigate and characterize materials of different heterogeneous structures on a micrometer (μm) range and also in nanometer (nm) scale. As we can get an idea from the name of this spectroscopy, the image is formed by scanning (rastering) the surface of the specimen line by line using beam of electrons. This technique can be used to investigate thick specimens as there's no need for electron to transmit in the sample. The concept

of SEM was first described by Knoll in 1935 but the device was first constructed by Zyworkin in 1942.

4.7.1 Components of SEM

The microscope construction can be divided into three main parts:

1. The specimen chamber

2. The electron optics system

3. Acquisition system, electronics

4.7.1.1 Specimen Chamber

The specimen chamber contains the stage on top of which the specimen is placed. The stage is able to move in different directions, such that in x,y and z direction. The optical system is placed above the specimen and the electron ray is generated and focused there. The acquisition system have a set of detectors which collects specific type of signals, secondary and back-scattered electrons, and convert the signal into pixel intensities. All the components of this device operates in high vacuum [22].

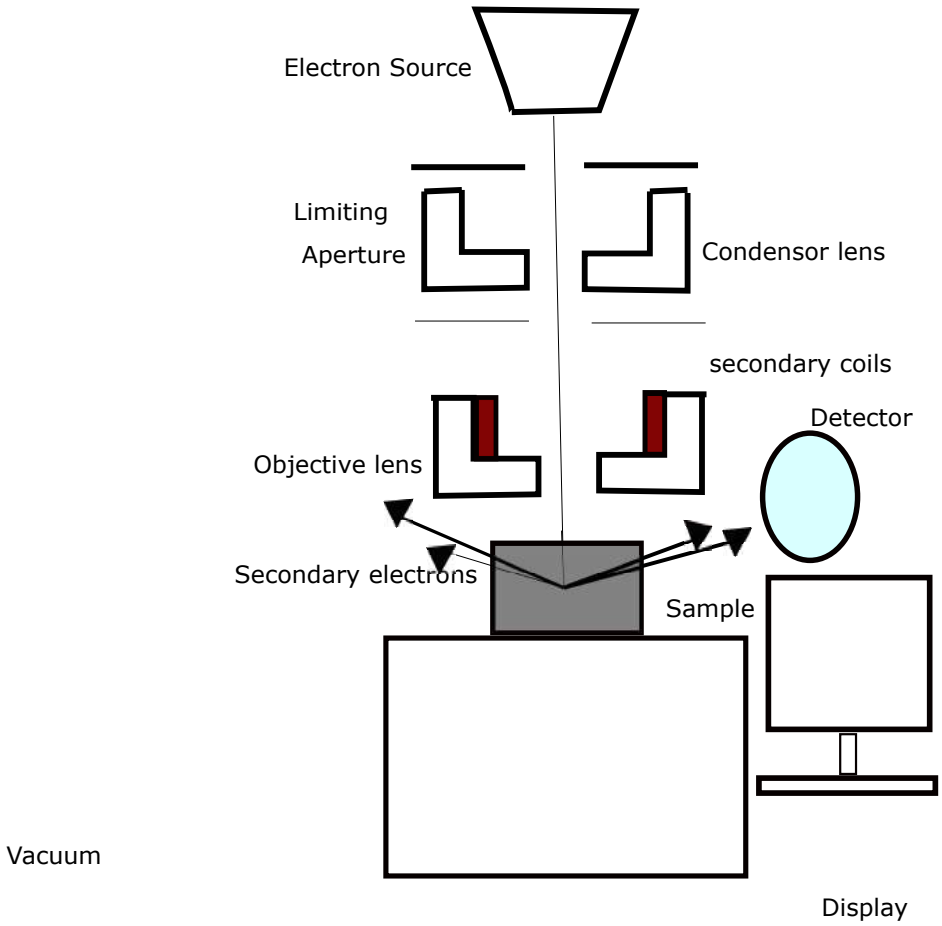

Figure 4.10: Schematic of Scanning-Electron-Microscope (SEM) with all of the basic components which includes condensor lens, electron source, objective lens, detector and a screen to display.

The electron optics is the most vital component of this system. It is composed of electron gun, condenser lens, deflection system and objective lens. The electron gun generates the beam of electrons by accelerating them by applying higher energies between 2 and 1000 keV. The energy at which these electrons are accelerated impacts on the brightness of the final image that is formed. This raw beam should be itself demagnified in order for it to hit at specific positions or to follow the line by line sample scanning process. Demagnification is the process in which the diameter of the ray reduces, and this is done by the condenser lens (electron lens) otherwise a blurry or small resolution image is formed. At second

place, coils are placed in order to deflect the beam on the discrete positions so that at each certain point, intensity can be noted. The last component is objective lens to converge beam on the specimen. As the beam is naturally diverging in all directions, a lens is needed to converge the ray at the end of the optical system.

When the beam hit the specimen, it interacts with it and electrons are scattered either elastically or in-elastically. If the thickness of the sample is less then e's may transmit from the sample un-absorbed and image is created of TEM, if the width of sample is thicker then e's can't pass through it and and these surface particles gives information about SEM. Those electrons which are ejected from the specimen as a result of inelastic scattering are referred as secondary electrons and can be recorded to form an image of the surface of the scanned object. In-elastically scattered electrons carry more energy and form an image which carries more information about the material composition of the specimen as shown in the figure 4.10. Generally, the computer software shifts the stage as it shifts from one position to another.

4.7.2 Surface Morphology

SEM can give data on synthetic structure, surface topography and crystalline structure of the specimen. SEM enjoys upper hand over optical microscopy which incorporates enormous depth such that majority of the sample area is simultaneously in focus of image whatever the surface harshness is. Much higher magnification can be achieved with ultimate resolution of 1 nm.

4.7.3 Types of Electron Images

"Secondary electron images", these electrons escape from the specimen with the energies beneath 50eV mainly knocked out of their shells around an atom by some incident electron. These give the most noteworthy spatial resolution images as they can escape from a shallow and signals comes from a space about the size of the electron probe.

"Back scattered electron images", are those in which interacts with the nucleus of the atom such that to scatter from a large angle and re emerge from the surface. They have slightly less resolution as compared to secondary electrons.

"Auger electrons and X-rays" are radiated from the atomic layer that is near to the surface. These characteristic x-rays are produced by atoms when the high energy particle knocks out an inner shell electron and outer shell electron moves inwards to fill the vacancy.

4.8 Energy Dispersive X-ray(EDX)

Energy dispersive spectroscopy is a strategy for compound micro analysis of a material. The hardware utilized for this technique is Scanning Electron Microscope (SEM), which is introduced with a x-beam spectrometer. X-ray detector is the main component of EDX, which is a pulse processor to measure voltage pulses that comes from the beam of x-ray and giving their respective energies and a PC for recording the data.

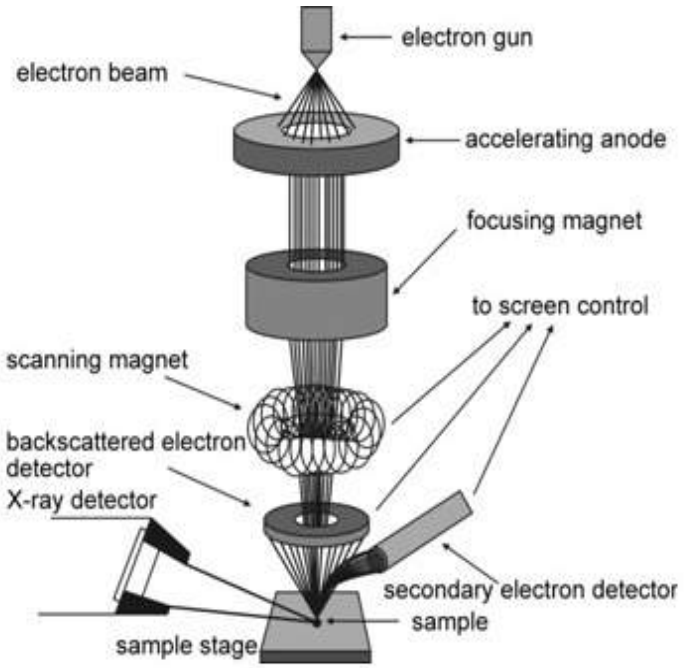

Figure 4.11: Schematic of Energy Dispersive X-ray (EDX). It is similar to the SEM and records the data with the help of same instruments as that of SEM.

4.8.1 Working Mechanism

$TiO_{2-x}N_y$ is barraged with a focused electron beam to such an extent that it creates auxiliary electrons or x-rays. The strong detector of the EDX gets the x-rays and creates current of limited quantity. Usually used Si detectors are "Lithium drifted Silicon" which are cooled with the assistance of liquid nitrogen. Next this is appended to an amplifier which converts the signal into voltage corresponding to the X-ray energies and amplifies the voltage.

The magnitude of the voltage pulse is in direct relation with the x-ray energy and the energy of the x-ray is comparing to every particular component from which it is discharged. The voltage signal is then ship off to the PC which gives the graph between voltage and time [23]. The data obtained is then analyzed and a spectrum of number of emitted rays vs energy is created. The atomic composition

can be determined from the spectrum. Each element has unique atomic structure which gives unique set of peaks on each element x-ray spectrum [24].

4.8.2 Generation of X-rays

EDX tells us about the basic creation of the material by understanding the x-ray energies. This continuum of x-ray beam is created because of the inelastic impact of SEM beam electrons with the sample. High energy beam electrons are incident on the sample with acquiring enough kinetic energy to conquer the binding energy of the specific inner K shell electron, it will knock the inner shell electron from the atom which after ionizes the atom. Binding energy is defined as energy required to ionize the atom and is also called as critical ionization energy. Striking of electron process continues such that when a vacancy is created then an electron jumps from higher shell to fill the space.The excess energy is emitted as characteristic x-ray energy i.e. in case of electron transition between two shells L and K ,it is written as:

$$E_x = E_k - E_l \tag{4.4}$$

K_α and K_β x-rays are produced when transitions of electrons occurs between L to K shell and from M to K shell, respectively. The intensity of the spectrum of K_β is higher than K_α as the energy difference between shells is greater. The empirical Moseley's law states that if K, L or M energy is known then the atomic number of the element can be determined. Elements with low atomic number(Z) will emit x-rays from K series , Intermediate Z elements will emit from L series [25].

The continuum of x-rays occurs (Bremsstrahlung) when the electron beam interacts with the electric field of the sample atom and lose kinetic energy which is emitted in the form of continuum x-rays. This can be observed as a background

in EDX spectrum [26]. The wavelength and energy of the x-ray can be expressed by Eq. (4.5):

$$\lambda = \frac{hc}{E} \tag{4.5}$$

where:

c is speed of light, λ has units of nm and energy has units of Kev.

4.9 Ellipsometry

"Surface Ellipsometry" is non-destructive and simple method in field of light(optical) interaction to extract extensive amount of information about the optical pattern with correct ellipsometric models applied to fit the data that is measured. The VASE M2000F rotating compensator ellipsometer (RCE) measured the angles ψ and δ with wavelength on the x axis. It depends on polarizing quantities with suitable manipulation of measured data, it consists of light source, a retarder, a linear polarizer, sample, analyzer and detector. The arm that is connecting source, polarizer and retarder prepares a known polarization of light that is incident on the sample. The other arm that is connecting analyzer and detector is to observe the change in polarization produced by the sample as shown in the figure 4.12

Ellipsometry has been exploited as a unique research tool to determine the optical properties of materials in a noninvasive and non-contact manner with a high degree of accuracy. The real and imaginary parts of the complex dielectric function of a material can be determined directly without the inversion of Kramer's Kronig relation using this technique [3].

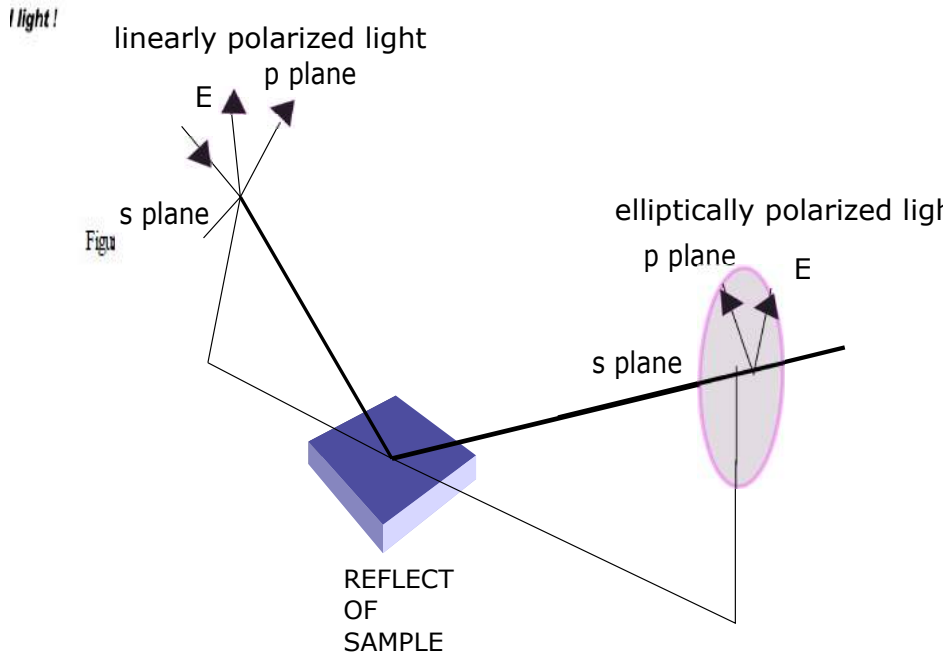

Figure 4.12: Schematic of the working mechanism of Ellipsometry. It includes linearly polarized light which is incident on the sample and changes it's phase to elliptical polarized light.

4.9.1 Working Principle

In this optical technique, the specimen is illuminate to beam of light. The incident light on the sample is already polarized as shown in the figure 4.12 Three fundamental benefits of ellipsometry on basis of reflection and transmission measurements are:

1. Precision: The modification in the polarization state of the light is because of the way that in unlimited intensity measurement, ellipsometry is not delicate to change. In this way, it very well may be specific without knowing "absolute" intensity values.

2. Sensitivity: Provides information about the phase analysis and thickness of different layers of thin films.

3. Information: Amplitude and phase angle information on each wavelength can be extracted.

Ellipsometer (α-SETM J.A Woollam co. Tno) is utilized for measuring thickness of thin films. Different optical parameters like, refractive index, extinction, absorption coefficient, epsilon and band gap values were extracted as a function of wavelength using the spectroscopic Ellipsometry technique.

4.10 Raman Spectroscopy

Raman spectroscopy is basically a technique that is analyzed for the study of the raman effect. Such technique is well-known due to the inelastic scattering of the light that is incident though a laser source. In an inelastic scattering, frequency of the monochromatic light photon changes, after its interaction with the sample. Light photons from particular monochromatic laser beam are firstly absorbed by the sample and then get re-produced after a very short period. As a result, this re-emitted photon's frequency either shifts up or down in compared with the original frequency, such shifting in the frequency is called raman shift.

Moreover, this frequency shift provides us the information about the transitions like rotational, vibrational and about other low frequency transitions in molecules. In other words, when the light interacts with the phonons or the molecular vibration, the inelastic scattering occurs and frequency of incident light changes and this change in frequency provides the information about the different modes of given material. However, this technique can be employed to study samples

in the solid, gaseous and the liquid form as well. A raman spectrometer usually

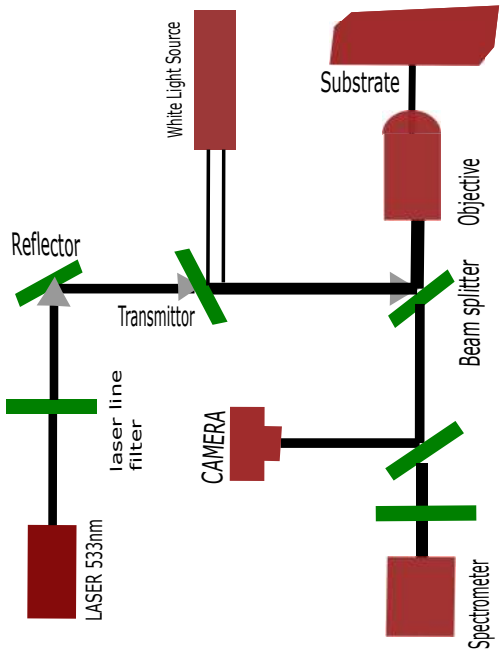

Figure 4.13: Schematic of RAMAN Spectroscopy with it's components laser beam, reflector, transmittor, spectrometer etc.

comprises as shown in the figure 4.13, the following four key modules:

1. Illumination system with the light collection optics.
2. Laser
3. Wavelength selector (notch filter)
4. Detector

Normally, the sample is irradiated with the laser beam which lies in ultraviolet, visible or near infrared region. The dispersed light beam is further collected through a lens and passes via filter to separate the wanted raman modes which are to be detected. Moreover, the light from Rayleigh-scattering is produced mainly due to grating quality and processed dispersion of light by the gratings.

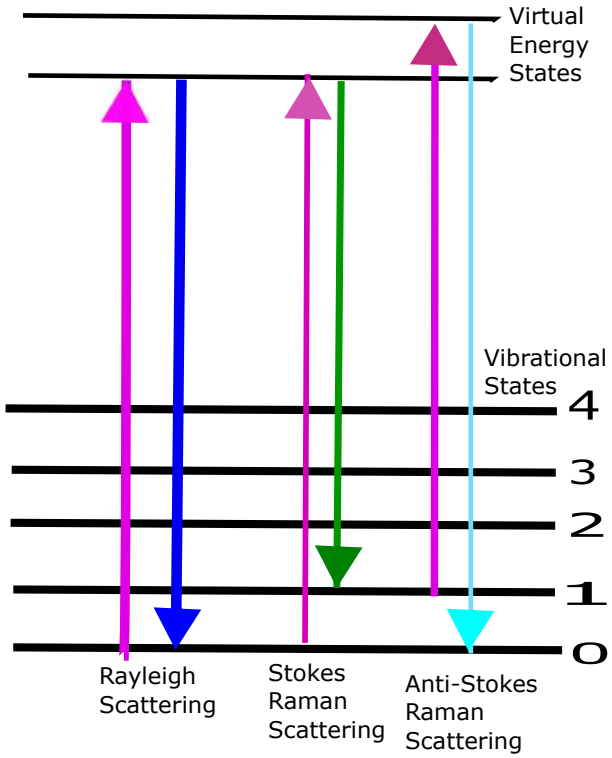

Figure 4.14: Rayleigh Scattering, Stokes raman scattering and Anti-Stokes raman scattering between different energy level states in Raman Spectroscopy.

4.10.1 Raman Effect

Raman Effect inside materials is based on their molecular distortions. The monochromatic light beam is an oscillatory electromagnetic wave having an electric field vector. Interaction of electromagnetic waves with sample induces an electric dipole moment which induces a deformation. Due to the periodic nature of incident waves, the induce deformation will be periodic and hence the molecules begin vibration with specific frequency. Molecules of the material are excited by the incident laser frequency and then get transformed into oscillating dipoles. Hence, following three different kinds of light frequencies are emitted by these oscillatory dipoles as shown in the figure 4.14

4.11 Photoluminescence

Photoluminescence (PL) is defined as the spontaneous light emission from any sample under the UV / VIS excitation that occurs from electronic excited states consequently. PL is considered as preferable technique for investigating the electronic structure of different materials because it is a non-destructive, contact-less method.

4.11.1 Components of PL

The instrumentation required for ordinary PL working is simple:

1. optical source
2. spectrometer
3. detector

The sample is usually excited with the He-Cd laser. By the absorption of photon, the electrons inside the molecular states of the sample get into the corresponding excited states. When the electrons in these excited states come to their ground state, they emit the photon again which are further detected by the amplifier for the output signal in the form of spectrum. Hence, PL is the process in which the materials absorb the photons and re-radiate them by converting UV and VIS light into the various coloured luminous emission with after-glow for the calculated duration.

However, in comparison with the other optical methods of the characterization like in the reflection and the absorption study, PL is less strict concerning the alignment of beam, sample thickness and surface flatness. PL is normally characterized for investigating the semiconductor. When sample is usually exposed

to visible light radiation, atoms in such sample enter its excited states. When these atoms return toward lower energy states, they emit radiations and the luminescence spectrum is studied. PL can be obtained at the room temperature, but at low temperatures, the spectral lines get relatively sharper and stronger, by allowing more structure assembly to be revealed.

Chapter 5

Results and Discussion

5.1 Electronic properties

5.1.1 Simulations

The electronic properties were studied for nitrogen doped TiO_2 structure. DFT calculation shows that nitrogen is induced as a dopant for the formation of the localized state in the band gap. Density of states by substitutional doping of nitrogen lies exactly in the region between conduction band and valence band and that is band gap and above the valence band while by doing interstitial doping it lies little higher in the band gap. Absorption edge shifts towards lower energies(visible region) when it is excited from these states to conduction band. This is observed in nitrogen doped TiO_2 with respect to undoped TiO_2. The nitrogen incorporation in structure might produce oxygen vacancies which consequently reduce the energy. Due to the doping, there's a reduction in energy which forms oxygen vacancies.

By doing Simulation while using mbJ approximation, we can say that the band gap of undoped TiO_2 found out to be 2.6eV. Then by doping, band gap reduces

to the value of 1.2 eV such that the e's from the lower band(VB) jumps to the upper band(CB) and occupies states and CB states comes in the region of band gap.

5.1.1.1 Density of States(DOS)

5.1.1.1.1 Undoped TiO_2

The respective positions of DOS are arranged by referencing to the core levels of the atom that is farthest from the impurity. The dotted line at zero (0 eV) presents the fermi energy(E_f).

Figure 5.1 shows the Total Density of States (TDOS) and Partial Density of States (PDOS) for undoped TiO_2 structure. TDOS figure 5.1a depicts a clear gap between the fermi level and the conduction state which is helpful for evaluation of band gap. The maximum of the peak of TDOS lies in the region of -3.8 eV to -4.3 eV in valence band and also there's a maxima of peaks in conduction band in 3.0 eV to 3.5 eV region where most of the electrons reside. Similarly, PDOS figure 5.1b of Ti reveals the maximum of the state at approximately 3.8 eV in conduction band. The maximum contribution of Ti atom arises from d-orbital of Ti atom. From figure 5.1c of PDOS of O atom, the valence band (VB) is mainly dominated by O 2p orbitals and the maximum of the peak lies at -4.4 eV in the valence band. Thus valence band is contributed by O atoms and conduction band is contributed by Ti atoms. The electron existing in the valence band can absorb more than 2.9 eV of energy and can excite to d orbital of conduction band. The peak in the PDOS located at -6 eV to -4 eV belongs to 2p orbitals of O atoms and is higher than the peak of Ti 2p states such that Ti s and p states makes negligible contribution in DOS spectra. Our purpose is to reduce the band gap value and to see the effect of doping.

Thus, from DOS spectra it can be observed that p-orbital of oxygen atom and d-orbital of Ti atom contributes to produce p-d hybridization in TiO_2 structure. In principle, the substitution of an element with different charge can induce charge imbalance, resulting in the formation of a crystallographic point defect, such as oxygen or titanium vacancy.

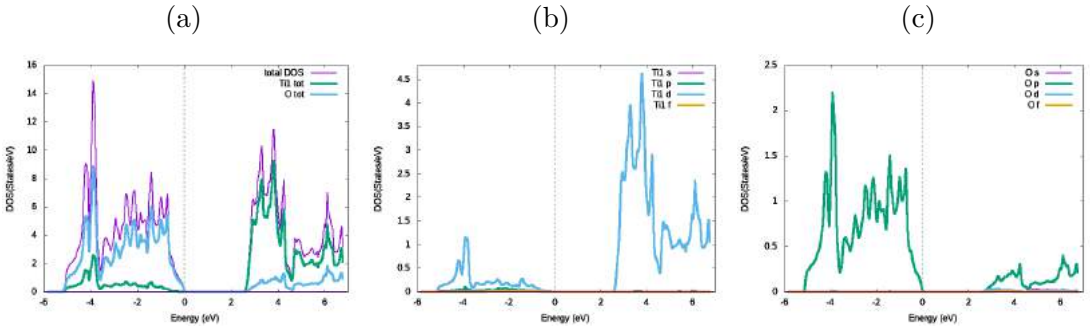

Figure 5.1: Density of states of TiO_2 a) TDOS and (b-c) PDOS spectra of Ti and O atoms, respectively.

5.1.1.1.2 12.5% N doped TiO_2

Figure 5.2 shows the Total Density of States (TDOS) and Partial Density of States (PDOS) for 12.5% N doped TiO_2 structure. TDOS figure 5.2a depicts gap between the fermi level and conduction state. The maximum of the peak of TDOS lies in the region of -4.6eV to -5.0eV in valence band and also there's a maxima of peaks in conduction band around 3.1eV where most of the electrons reside. Similarly, PDOS figure 5.2b of Ti reveals the maximum of the state at approximately 3.0 eV in conduction band. The maximum contribution of Ti atom arises from d-orbital of Ti atom. From figure 5.2c of PDOS of O atom, the valence band (VB) is mainly dominated by O p orbitals and the maximum lies at -4.4 eV in valence band. From figure 5.2d of PDOS of N atom, the VB is mainly prominent by N p orbitals with maxima lies at fermi level which indicates the overlapping of corresponding states. The electrons mostly reside near fermi level

in N PDOS. Thus valence band is contributed by O and N atoms and conduction band is contributed by Ti atoms. The electron existing in the valence band can absorb more than 1.4 eV of energy and can excite to d orbital of conduction band. Thus, from DOS spectra it can be observed that p-orbital of oxygen and nitrogen atom and d-orbital of Ti atom contributes to produce p-d hybridization in 12.5% N doped TiO_2 structure.

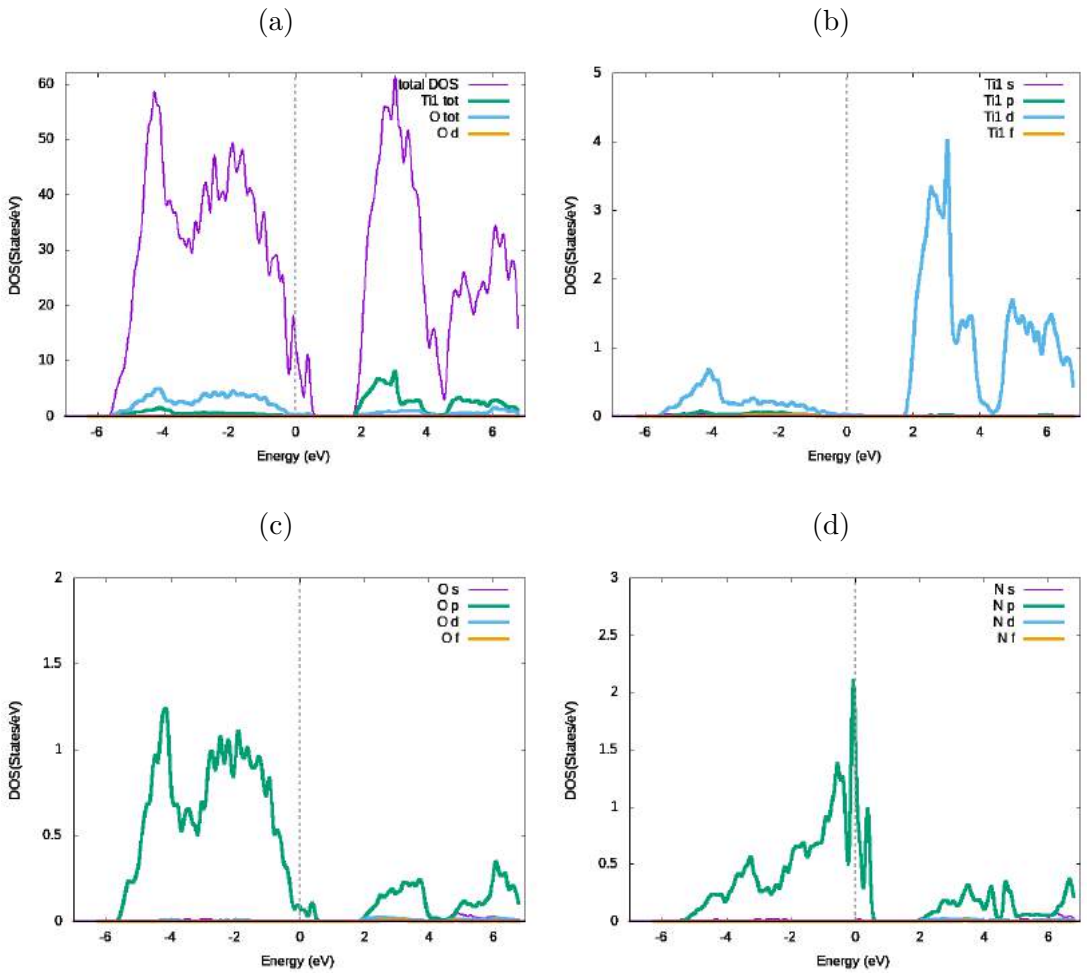

Figure 5.2: Density of states of TiO_2 and N doped TiO_2(a) TDOS and (b-d) PDOS spectra of Ti, O and N atoms, respectively.

.

5.1.1.1.3 25% N doped TiO_2

Figure 5.3(a-c) depicts the Total Density of States (TDOS) and Partial Density of States (PDOS) for 25% N doped TiO_2 structure. TDOS figure 5.3a depicts a clear gap between the fermi level and conduction state. The maximum of the peak of TDOS lies in the region of -4.8eV to -5.2eV in valence band and also there's a maxima of peaks in conduction band in 3.0eV to 4.0eV region. Similarly, PDOS figure 5.3b of Ti reveals the maximum of the state at approximately 3.0eV in conduction band. The maximum contribution of Ti atom arises from d-orbital of Ti atom. From figure 5.3c of PDOS of O atom, the valence band (VB) is mainly dominated by O p orbitals and the maximum lies at -4.3 eV in valence band. From figure 5.3d of PDOS of N atom, VB is mainly prominent by N p orbitals with maximum lies at 0 eV in valence band. The electrons mostly reside near fermi level in N PDOS. Thus valence band is contributed by O and N atoms and conduction band is contributed by Ti atoms. The electrons existing in the valence band can absorb more than 1.4 eV of energy and can excite to d orbital of conduction band. The peak in the PDOS graph located at -6 eV to -4 eV belongs to p orbitals of O and N atom and is higher than the peak of Ti p states. The states are shift towards CB because of 25% doping of nitrogen content such that increasing conduction of the structure.

Thus, from DOS spectra it can be observed that p-orbital of oxygen and nitrogen atom and d-orbital of Ti atom contributes to produce p-d hybridization in 25% N doped TiO_2 structure.

5.1.1.1.4 50% N doped TiO_2

The element N exists in the same column as Ti in the periodic table. The respective locations of DOS are adjusted by pointing to the respective core levels of the

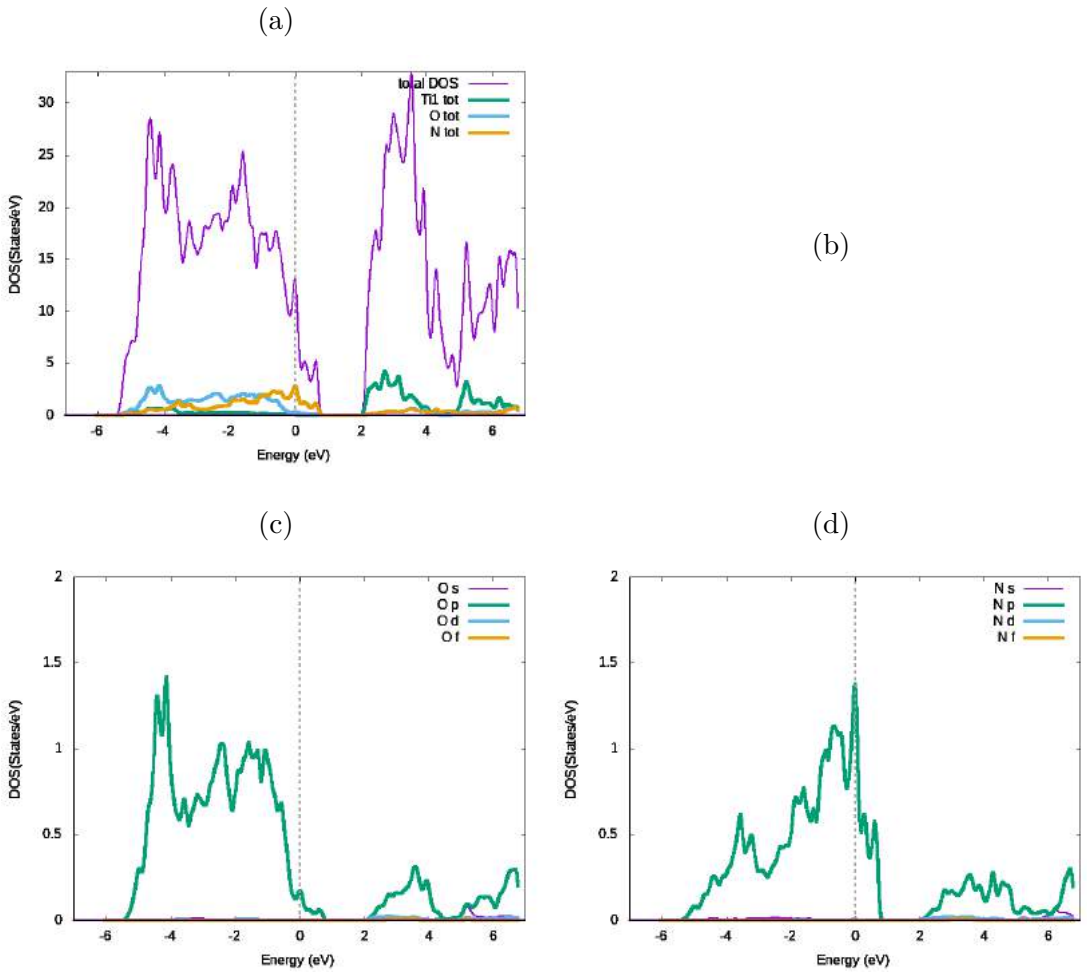

Figure 5.3: DOS of TiO_2 and 25% N doped TiO_2 (a) TDOS (b-d) PDOS spectra of Ti, O and N atoms, respectively

.

atom. Figure 5.4 shows the TDOS and PDOS for 50% N doped TiO_2 structure. TDOS figure (5.4a) depicts a clear gap between the fermi level and the conduction state. The maximum of the peak of TDOS lies in the region of -4.8 eV to -5.5 eV in valence band and also there's a maxima of peaks in conduction band in 3.3eV to 4.5eV region. Similarly, PDOS figure 5.4b of Ti reveals the maximum of the state at approximately 3.6 eV in conduction band. The maximum contribution of Ti atom arises from d-orbital of Ti atom. From figure 5.4c of PDOS of O atom, the valence band (VB) is mainly dominated by O p orbitals and the maximum

lies at -4.8 eV in valence band. From figure 5.4d of PDOS of N atom, VB is mainly prominent by N p orbitals with maximum lies at -4.1 eV in valence band. Thus valence band have O and N atoms and conduction band have Ti atoms. The electron existing in the valence band can absorb more than 1.2 eV of energy and can excite to d orbital of conduction band. The states are shift towards CB because of 50% doping of nitrogen content such that increasing conduction of the structure.

Thus, from DOS spectra it can be observed that p-orbital of oxygen and nitrogen atom and d-orbital of Ti atom contributes to produce p-d hybridization in 50% N doped TiO_2 structure.

5.1.1.1.5 83.5% N doped TiO_2

Figure 5.5 shows the TDOS and PDOS for 83.5% N doped TiO_2 structure. TDOS figure 5.5a depicts gap between the fermi level and conduction state. The maximum of the peak of TDOS lies in the region of -0.9 eV to -1.9 eV in valence band and also there's a maxima of peaks in conduction band around 3.9 eV. Similarly, PDOS figure 5.5b of Ti reveals the maximum of the state at approximately 3.0 eV and 5.0 eV in conduction band. The maximum contribution of Ti atom arises from d-orbital of Ti atom. From figure 5.5c of PDOS of O atom, the valence band (VB) is mainly dominated by O p orbitals and the maximum lies at -4.4 eV in valence band. From figure 5.5d of PDOS of N atom, VB is mainly prominent by N p orbitals with maximum lies at -1.3 eV in valence band. The PDOS of N atom shifts towards valence band region as the concentration or amount of nitrogen increases in the structure. Thus valence band is contributed by O and N atoms and conduction band is contributed by Ti atoms. The electron existing in the valence band can absorb more than 1.0 eV of energy and can excite to d orbital

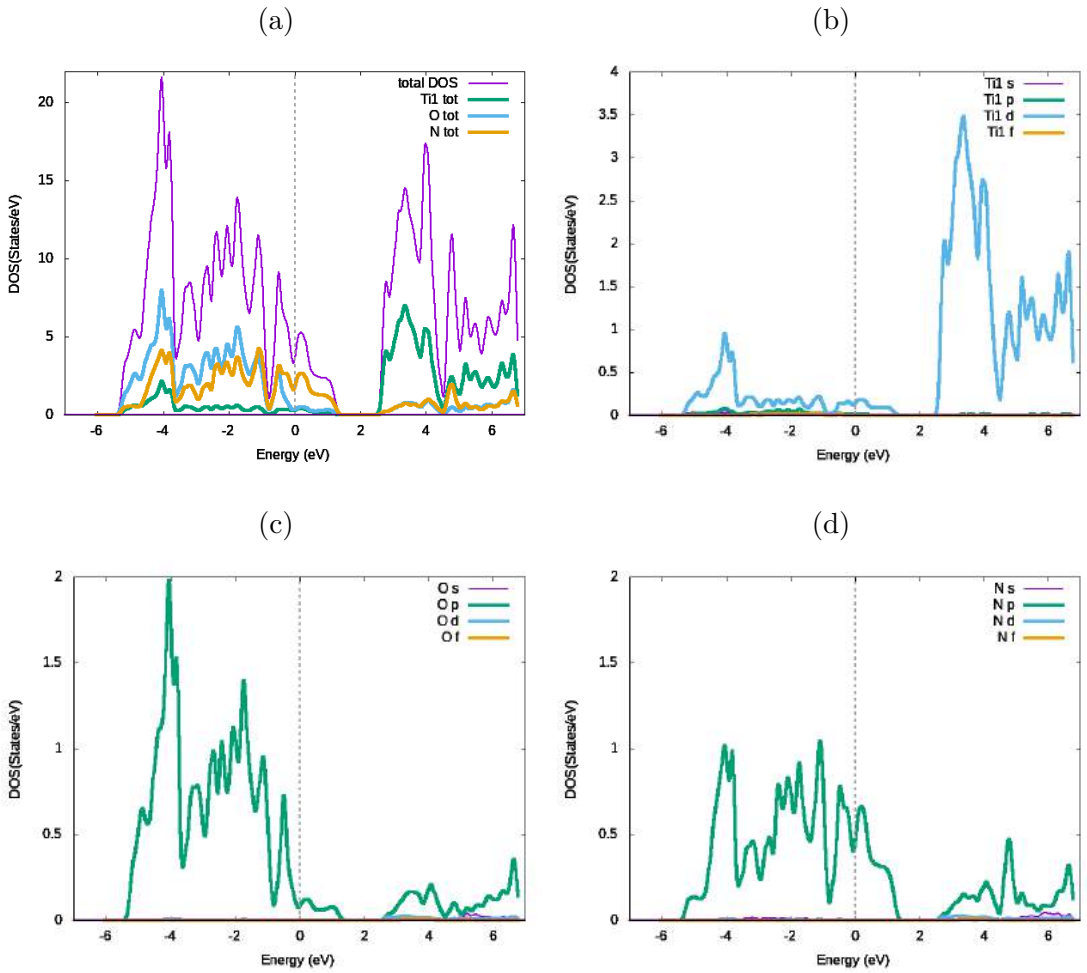

Figure 5.4: DOS of TiO_2 and 50% doped TiO_2(a) TDOS and (b-d) PDOS spectra of Ti, O and N atoms, respectively

.

of conduction band. This is the lowest band gap with maximum conductivity. .

5.1.1.2 Band gap structure of TiO_2

In reciprocal space, there are two parameters and that are energy and momentum, the relation between these two quantities is termed as band structure. It provides information about the multi terms such as band gap or effective mass of charge carriers. Furthermore dispersion relations can be related to the peak positions of the dielectric function in order to have understanding of the optical transition

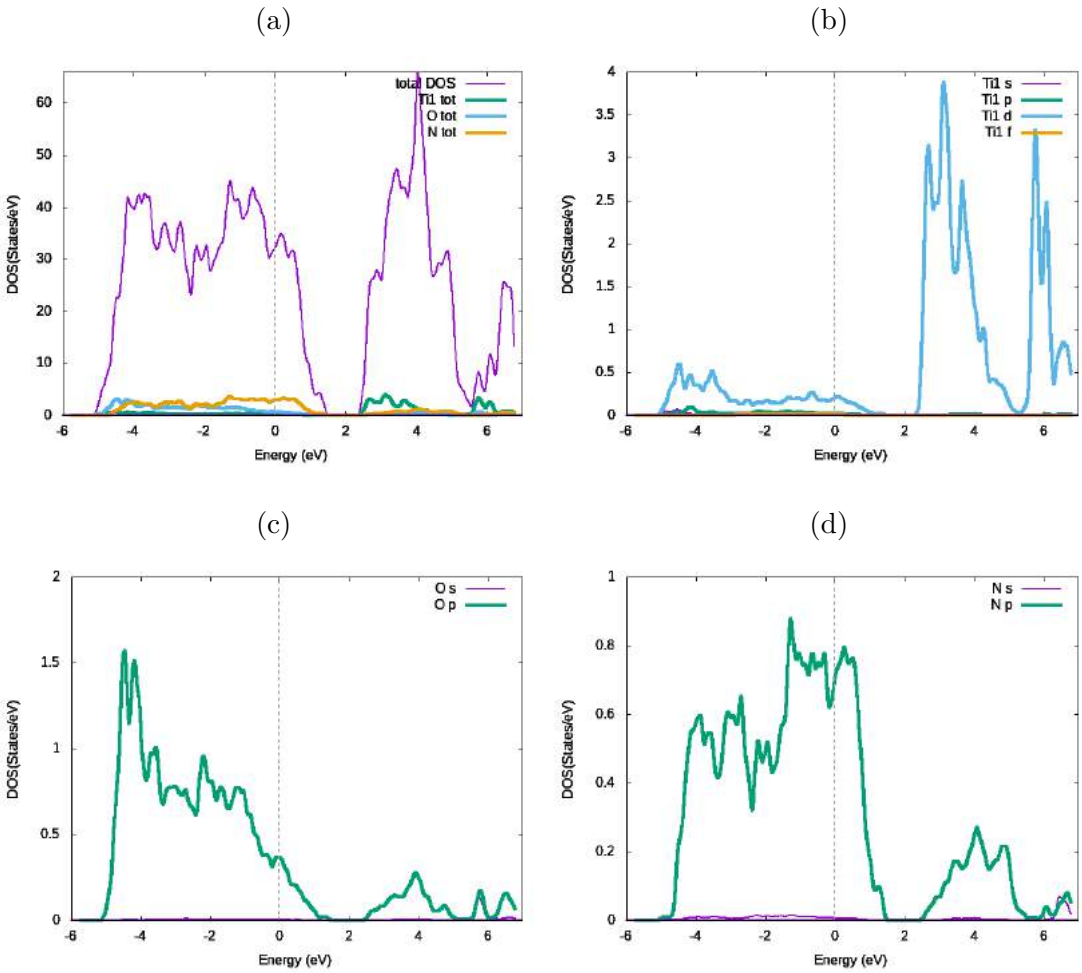

Figure 5.5: DOS of TiO_2 and 83.5% N doped TiO_2(a) TDOS and (b-d) PDOS spectra of Ti, O and N atoms, respectively

.

between different states. In Brillioun zone, band structure is calculated along the direction of high symmetry. Maxima of the valence band lies at the Δ , σ etc points depicting the mobility of electrons along the specific orientation.

The band structure of pure TiO_2, N doped TiO_2 (12.5%, 25%, 50% and 83.5%) can be calculated by knowing the value of the band gap. The calculated band gap value is 2.6 eV for undoped TiO_2 which is close to the reported value.

E_f is showing line of fermi level which is at 0.0 eV. Undoped TiO_2 shows direct band gap at σ branch with value of 2.6 eV. 12.5% N doped TiO_2 shows 1.6 eV

band gap. It can be seen that states are overlapping in valence band are above fermi level due to doping. 25% N doped TiO_2 shows that the lowest of conduction band and highest point of valence band have a difference of 1.4 eV between these states. 50% N doped TiO_2 shows that there is a difference of 1.1eV between these states while 83.5% N doped TiO_2 shows that the lowest of conduction band and highest point of valence band have a difference of 1.0 eV between these states as shown in the figure 5.6. The overlapping of the states at fermi level in nitrogen containing composition is associated with the enhanced n-type conductivity due to nitrogen content.

5.1.1.3 Optical properties

Optical properties of materials can be calculated theoretically by using Kohn-Sham(KS) equations and experimentally through spectroscopic ellipsometry. Experimentally, Optical properties of Titanium Oxynitride TiN_xO_y can be investigated by calculating the various parameters like refractive index (n), Extinction Coefficient (k), Real part of Epsilon (ϵ), Reflectivity, Absorption Coefficient (α) and many more [27].

5.1.1.3.1 Real Epsilon(ϵ)

Generally, optical properties are being described by complex dielectric function ϵ (ω) such that it is explained as shown in Eq. 5.1:

$$\epsilon(\omega) = \epsilon_i(\omega) + \epsilon_j(\omega). \tag{5.1}$$

This property of epsilon depicts the material's capability to demonstrate polarization when material is illuminated with the incident light. The ϵ_r (ω) of the dielectric constant is obtained through the Krammers-Kronig transform while the

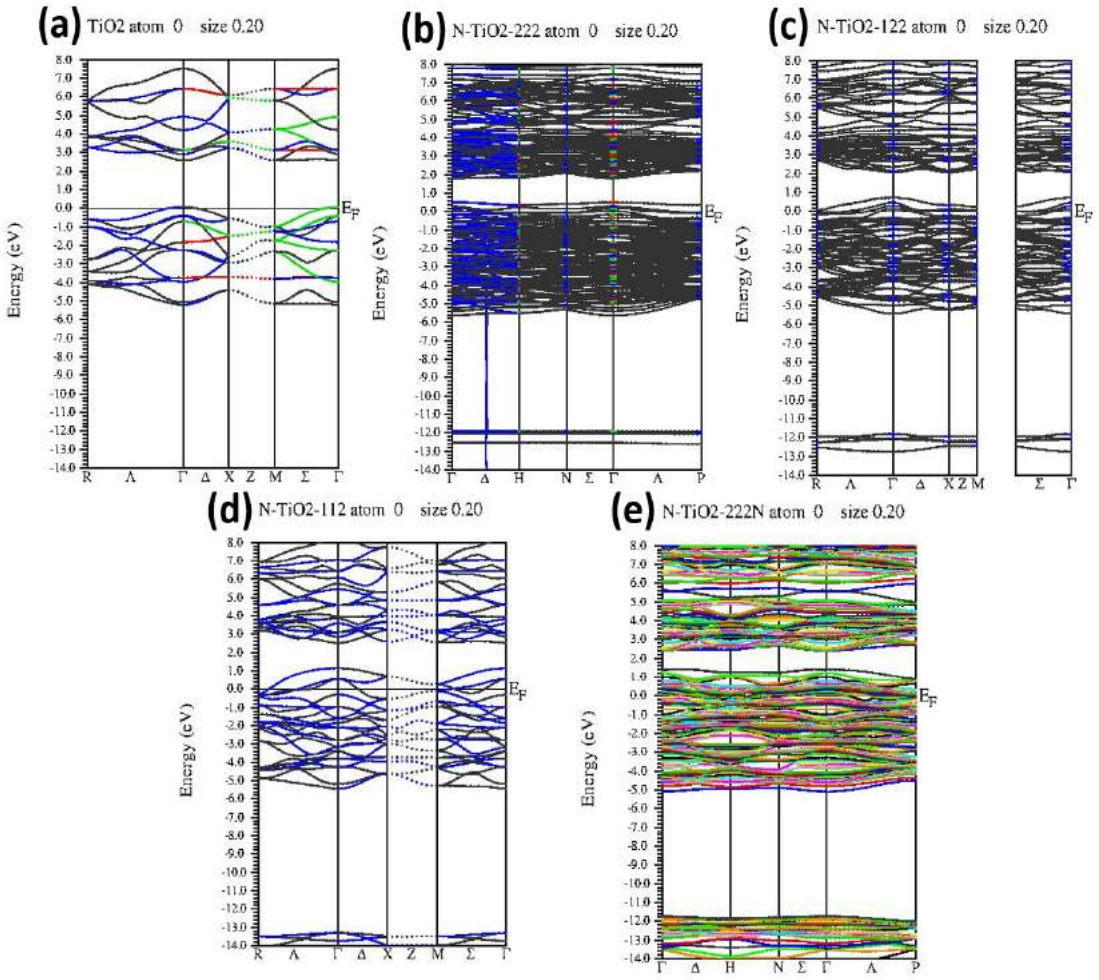

Figure 5.6: (a) Band structure of Undoped Ti_O2, (b) refers to 12.5% N doped Ti_O2, (c) refers to 25% N doped Ti_O2, (d) refers to 50% N doped Ti_O2 and (e) refers to 83.5% N doped Ti_O2

direct solution of the many body wave function yields the imaginary part ϵ_i (ω) of dielectric constant as in Eq. 5.2

$$\epsilon_r(\omega) = 1 + \frac{2}{\pi}\rho_o \int_0^\infty \frac{\omega' \epsilon_i(\omega)}{\omega' 2 - \omega^2}\, d\omega. \tag{5.2}$$

The dielectric behavior of a material is of great importance as other optical properties like refractive index, extinction coefficient, absorption coefficient, reflectivity [28]. Atoms can absorb energies at specific frequencies and can do tran-

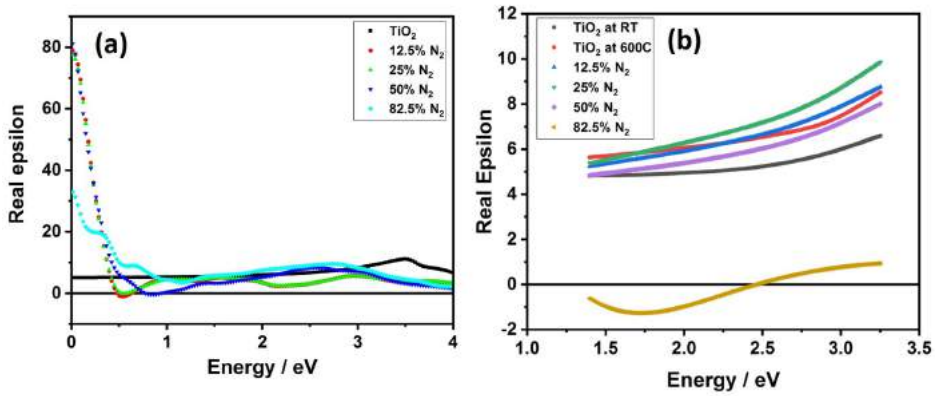

Figure 5.7: Graphs of Real part of epsilon: (a) Simulation of Undoped TiO_2, 12.5% , 25% ,50% and 83.5% N doped TiO_2 (b) Experimental graph of Undoped TiO_2, 12.5% , 25% ,50% and 83.5% N doped TiO_2

sitions between different orbitals of it's structure caused by resonant frequency. The value of epsilon at zero energy is called as static dielectric.

1. The real part defines the phase lag between frequencies i.e. how fast light moves in a material which describes the response of refractive index to the corresponding energies.

2. The imaginary part is related to the damping factor and it defines the absorption of radiations or loss of energy.

Figure 5.7(a) presents the theoretically obtained response of real part of dielectric constant for the energy range 0-4eV. Static value of dielectric constant increase with the increment of nitrogen content in structure attributed to the formation of defects in structure because nitrogen not only occupies the substitutional sites but also resides the interstitial positions in structure. ENZ behavior in the energy range 0-3eV becomes prominent in the compositions having higher contents of nitrogen depicting the transition of structure from semiconductor to semi-metallic and then metallic composites. One of the reason of obtaining various optical properties is because of variance in the level of residual oxygen that is flown as a

background vacuum.

When the level of residual oxygen increases than the corresponding temperature, then the thin films were fabricated. Because it exhibits a non-metallic behavior (TiO_2-like) by decreasing the oxygen concentration in the background. And it shows metallic (TiN) like behavior when the ENZ has the values ranging from 0 to 3 eV.

In this method, there is mixing of two phases such as TiN and TiO_2 phases in the presence of residual oxygen medium, a Maxwell-Garnet mechanism has been developed to simulate experimentally observed optical properties. In this model, oxynitride films were treated as composites of different phases, and effective dielectric constants were calculated.

There were two procedures that were going on:

1. TiO_2 inclusions in TiN films.

2. TiN inclusions in TiO_2 films.

TiN inclusions have plasmonic polarizibility while TiO_2 don't. This must be noted that in both of the cases, the presence of TiO_2 for high Titanium Nitride content appears as red shift to the ENZ point. There was no ENZ behavior observed in compositions having low nitrogen content contrary to the simulation results. Simulation result reflects the calculations for exact substitution of nitrogen in structure while in case of experimental findings we observed the formation of different composite phases.

These phases are attributed to the presence of major non-metallic contributions for lower contents of nitrogen. However, ENZ behavior achieved only for highest content of nitrogen reveals the presence of major metallic TiN phase in structure with minimal contribution of other non- metallic phases.

Pressure variation of N_2 gives information about the growth (saturation) of TiN

films. And if we decrease the percentage of nitrogen in our mixture then it'll give us some iformation about the phases of saturated TiN which are the source of producing TiN, TiNxOy and TiO_2 phases. And it's solely because of the change in the growth of residual oxygen as shown in the figure 5.7. If we change the percentage of gas mixture which has been deposited then we can basically manage the percentages of the three phases TiN ,TiO_2 and TiOxNy.

These thin films exhibit epsilon-near-zero values at certain frequencies. By increasing the amount of energy from the UV regime the partial pressure of nitrogen decreases. It also decreases the real part of the dielectric constant of the samples which are fabricated at room temperature and it remains negative (less than 2.5eV) and becomes positive after 2.5 eV. [29]

The real part of the dielectric constant shows a continuously decreasing trend with the increase in the value of energy that is exactly correlated with the trend of dielectric energy curves with negative values in both visible and infrared regions. And this change is nearly in parallel to the TiN like materials at high temperatures. It is attributed to the behavior of TiOxNy phases in the films [30]. The ENZ behavior was successfully achieved after a number of fabrication attempts in thin films having the highest content of nitrogen.

5.1.1.3.2 Absorption Coefficient (α)

The response of absorption coefficient with variation in energy range 0-4 eV was recorded and presented in fig 5.8. The optical absorption may be calculated using the Eq. 5.3

$$\alpha(\omega) = \sqrt{2}[\sqrt{\epsilon_r^2(\omega) + \epsilon_i^2(\omega)} - \epsilon_r(\omega)]^{\frac{1}{2}}. \tag{5.3}$$

where:

ϵ_r and ϵ_i are the real and imaginary part of the dielectric constant as in Eq. 5.4.

$$\epsilon(\omega) = \epsilon_r(\omega) + \iota\epsilon_i(\omega) \tag{5.4}$$

Absorption coefficient graph obtained through simulations as shown in figure 5.8(a). It shows a significant increase in visible regime in higher nitrogen content compositions. Experimentally obtained graph as in fig 5.8(b) acquired data reveals some difference in trend due to the presence of different phases in structure. However, both simulation and experimental graphs reflects same behavior for compositions having highest saturated content of TiN phase.

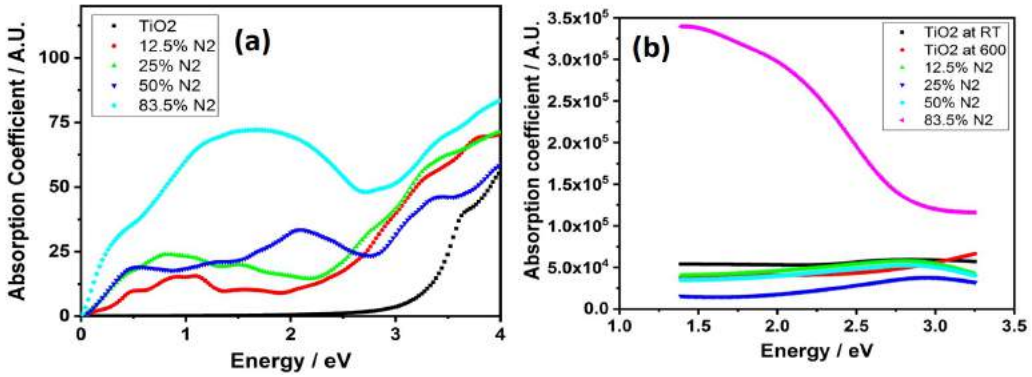

Figure 5.8: Graphs of Absorption Coefficient :(a) Simulation of Undoped TiO_2, 12.5% , 25% ,50% and 83.5% N doped TiO_2 (b) Experimental graph of Undoped TiO_2, 12.5% , 25% ,50% and 83.5% N doped TiO_2

5.1.1.3.3 Reflectivity

We can define reflectivity as: how much energy (of a particular wave) is being reflected from a surface on which it's going to incident. The reflectivity can be calculated using Eq. 5.5

$$R(\omega) = \left[\frac{\sqrt{\epsilon_1(\omega) + \iota\epsilon_2(\omega)} - 1}{\sqrt{\epsilon_1(\omega) + \iota\epsilon_2(\omega)} + 1}\right]^2 \tag{5.5}$$

The reflectivity variation with energy presents in fig 5.9(a) and figure 5.9(b) for simulations and experiment, respectively. The simulation data for reflectivity figure 5.9(a) shows an increasing trend for compositions having higher contents of nitrogen. Experimentally obtained data as in fig 5.9(b) reflects some variation in trend again due to the presence of composite phases in structure. However, highest values of reflectivity were observed in visible regime for different compositions for simulations as well as experimental outcomes.

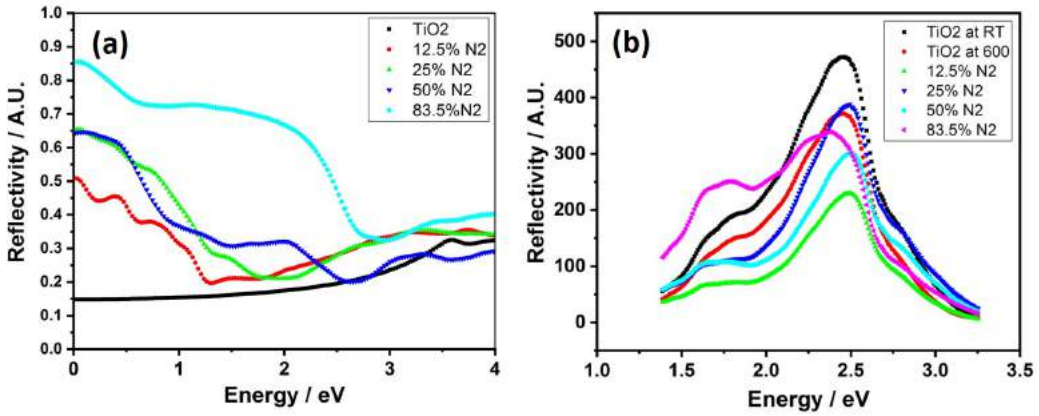

Figure 5.9: Graphs of Reflectivity :(a) Simulation of Undoped TiO_2, 12.5% , 25% ,50% and 83.5% N doped TiO_2 (b) Experimental graph of Undoped TiO_2, 12.5% , 25% ,50% and 83.5% N doped TiO_2

5.1.1.3.4 Refractive Index

Figure 5.10(a) and figure 5.10(b) presents the variation of refractive index as a function of energy for simulations and experiment, respectively. Simulation data figure 5.10(a) corroborates an exponential decrease in the refractive index values with increment of energy. Again experimental data in figure 5.10(b) reflects some alteration due to the facts described in previous sections.

It can be seen that optical constants are prominently affected by Oxygen flow rate or we can say that with the N/O ratio. The behavior of refractive index is changed between visible and infrared region. The refractive index n decreases

continuously with the Oxygen flow rate in the near infrared region and in the visible region it firstly increases and then decreases.

The knowledge of refractive index of any material illustrates the penetration of electromagnetic waves propagation through them. The refractive index (n) may be calculated using the formula as shown in Eq. 5.6:

$$\eta(\omega) = \left[\frac{\epsilon_1(\omega)}{2} + \frac{\sqrt{\epsilon_1^2(\omega) + \epsilon_2^2(\omega)}}{2}\right]^{\frac{1}{2}} \tag{5.6}$$

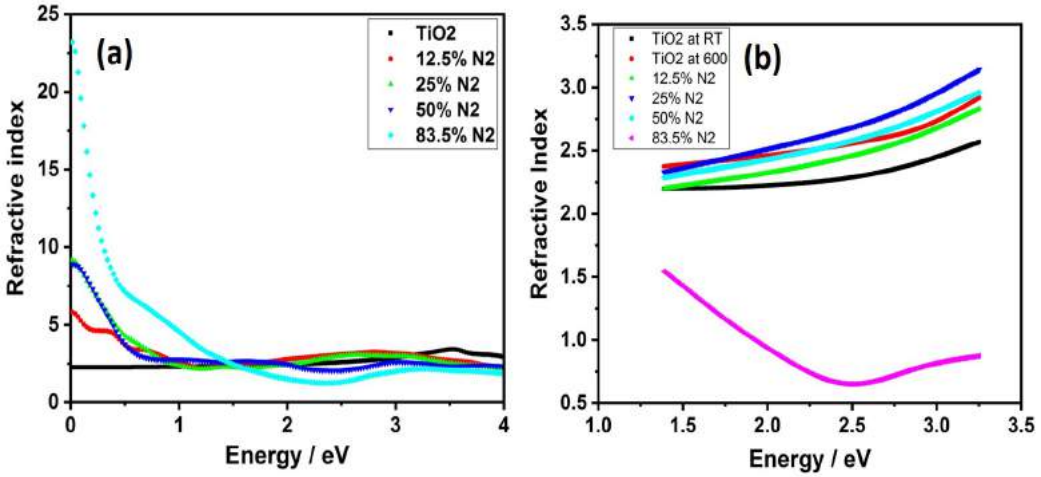

Figure 5.10: Graphs of Refractive index: (a) Simulation of Undoped TiO_2, 12.5% , 25% ,50% and 83.5% N doped TiO_2 (b) Experimental graph of Undoped TiO_2, 12.5% , 25% ,50% and 83.5% N doped TiO_2

5.1.1.3.5 Optical Conductivity (σ)

The optical conductivity $\alpha(\omega)$ may be calculated using the relation as in Eq. 5.7

$$\sigma(\omega) = -\iota\frac{\omega}{4\pi}\big(\epsilon(\omega) - 1\big) \tag{5.7}$$

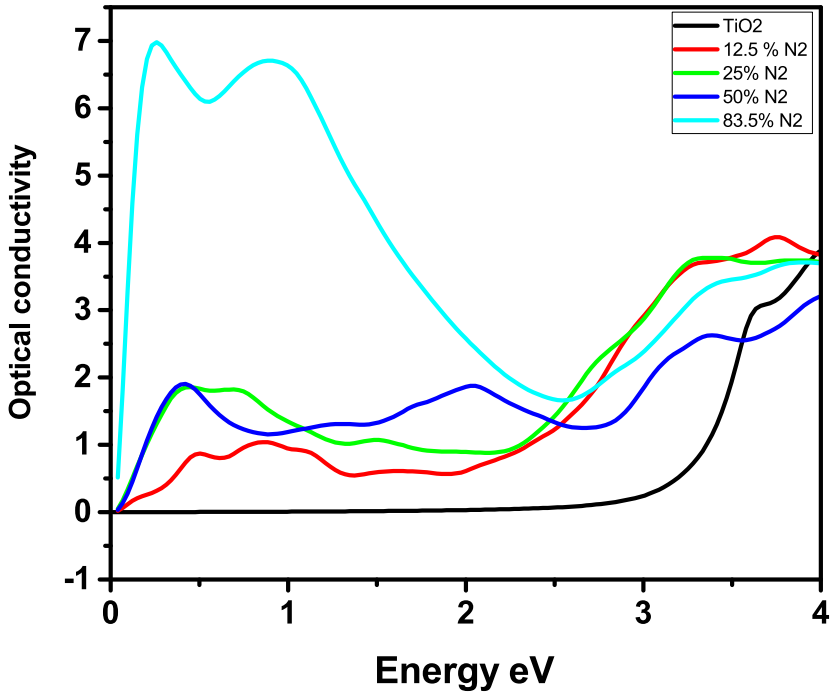

H

Figure 5.11: Simulation graph of Optical Conductivity of Undoped TiO_2, 12.5% , 25% ,50% and 83.5% N doped TiO_2

where:

$$k = \alpha\lambda/4\pi. \tag{5.8}$$

Optical conductivity shows an increasing trend with energy as shown in figure (5.11). A sharp increase in optical conductivity was observed in compositions with high content of nitrogen attributed to the localized overlapping states at fermi level as observed in DOS spectra [31].

5.1.1.3.6 Extinction Coefficient

Figure 5.12(a) and figure 5.12(b) presents the extinction response to energy for simulations and experimental observations, respectively. Extinction trend seems

similar for the composition having highest content of nitrogen and depicts an exponential decrease with energy. The contradiction between other simulation and experimentally obtained values for extinction is similar as described in the previous sections regarding different phase in case of experimental fabrication. Maxima of the extinction values of composition having highest nitrogen content was observed at lower energy ranges for both simulation and experiment as can be observed in extinction curves.

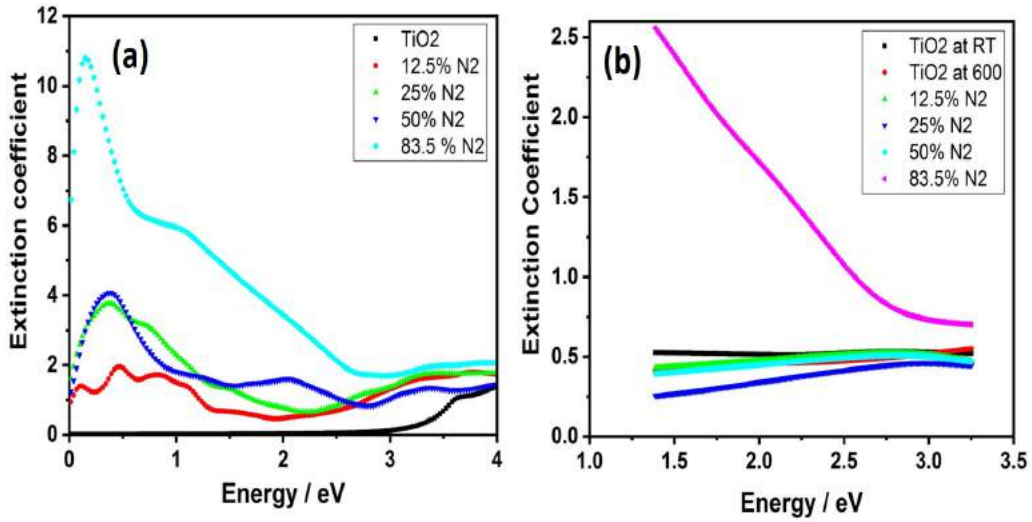

Figure 5.12: Graphs of Extinction Coefficient:(a) Simulation of Undoped TiO_2, 12.5% , 25% ,50% and 83.5% N doped TiO_2 (b) Experimental graph of Undoped TiO_2, 12.5% , 25% ,50% and 83.5% N doped TiO_2

By changing the flow rate of oxygen (O_2) , optical properties of $TiO_{2-x}N_y$ could be changed from metallic to semiconductor to dielectric. Optical constants of $TiO_{2-x}N_y$ films change due to the change in flow rate of O_2, which basically changes the electronic structure. When there's an interaction between the material and the incident light then: the optical properties of material are determined by the Interband and Intraband electronic transitions [32].

The electrons present in the d-band of Ti behave like the free electrons in TiN which means the electrons present in the conduction bands are portraying the

property of electrical conductivity. The electronic structure of TiN can be varied by inserting oxygen into the lattice points, which in result then gives tunable electrical and optical properties of $TiO_{2-x}N_y$ films. With the increasing concentration of oxygen, the contribution of the Interband transitions became more dominant and this occurs due to bound electrons, on the other hand the contribution of the Intraband transitions became less dominating [32]. When $TiO_{2-x}N_y$ films come in a state of oxygen-rich environment, the optical properties will be governed by the interband transitions, while the band gap will increase with the O concentration, which are characteristic property of semiconducting and insulating material [33].

5.2 Experimental Results

5.2.1 XRD

Figure 5.13 shows the XRD patterns for the TiO_2 and different concentrations of Nitrogen doped TiO_2 Thin films. figure 5.13a presents the XRD spectra of pure TiO_2 thin film grown at room temperature, which reveals the amorphous nature of the thin film as no peak is appeared in this spectra. Figure 5.13b shows the XRD pattern of TiO_2 thin films annealed at 600° C which confirms the clear rutile phase formation as XRD peaks appeared at corresponding angles. First peak is observed at $\theta = 26.208°$ with TiO_2 (110) plane , second peak at $\theta = 38.700°$ with TiO_2 (200) plane and third peak at $\theta = 54.833°$ with TiO_2 (211) plane. These peaks are matched from a reference card of TiO_2 which is associated with the rutile phase of Titania.

In forming thin films, there is a possibility of the peak observed of the substrate which is silicon in this case. Similarly, in figure 5.13c shows the XRD pattern of

Crystallite Size	
TiO_2 at 600∘	27.32
12.5% N TiO_2 at 600∘	0.68
25% N TiO_2 at 600∘	2.33
50% N TiO_2 at 600∘	0.93
83.5% N TiO_2 at 600∘	3.23

12.5% doped TiO_2 annealed at 600° C. The three peaks at same 2θ values are also observed in this pattern which convinces more about the rutile phase of the thin films. First peak is observed at $\theta = 26.158°$, second peak at $\theta = 38.700°$ and third peak at $\theta = 54.833°$. Rutile phase also observed in this case with some variation in intensity and shift of the XRD peaks. Moreover, in figure (5.13d), which is XRD pattern of 25% doped TiO_2 annealed at 600° C and reflects the formation of oxynitride phase as compared with standard data for oxynitride $TiO_{2-x}N_y$ crystal structure at $\theta = 33.896°$ with (302) plane. There is a sharp decrease in the intensities of TiO_2 phase. In figure 5.13e, the pattern of 50% doped TiO_2 annealed at 600° is shown. The peaks are observed again at same angles with slightly variations in the intensities of the peaks and in figure 5.13f, the pattern of 83.5% doped TiO_2 is shown and it shows one clear sharp peak of $TiO_{2-x}N_x$ at $\theta = 33.845°$ such that due to maximum content of nitrogen in the structure , this phase is dominated . XRD analysis hence confirmed the transition of TiO_2 rutile phase to oxynitride with increment of nitrogen content on structure.

The crystallite size is found using Scherrer's formula and is defined in the table below:

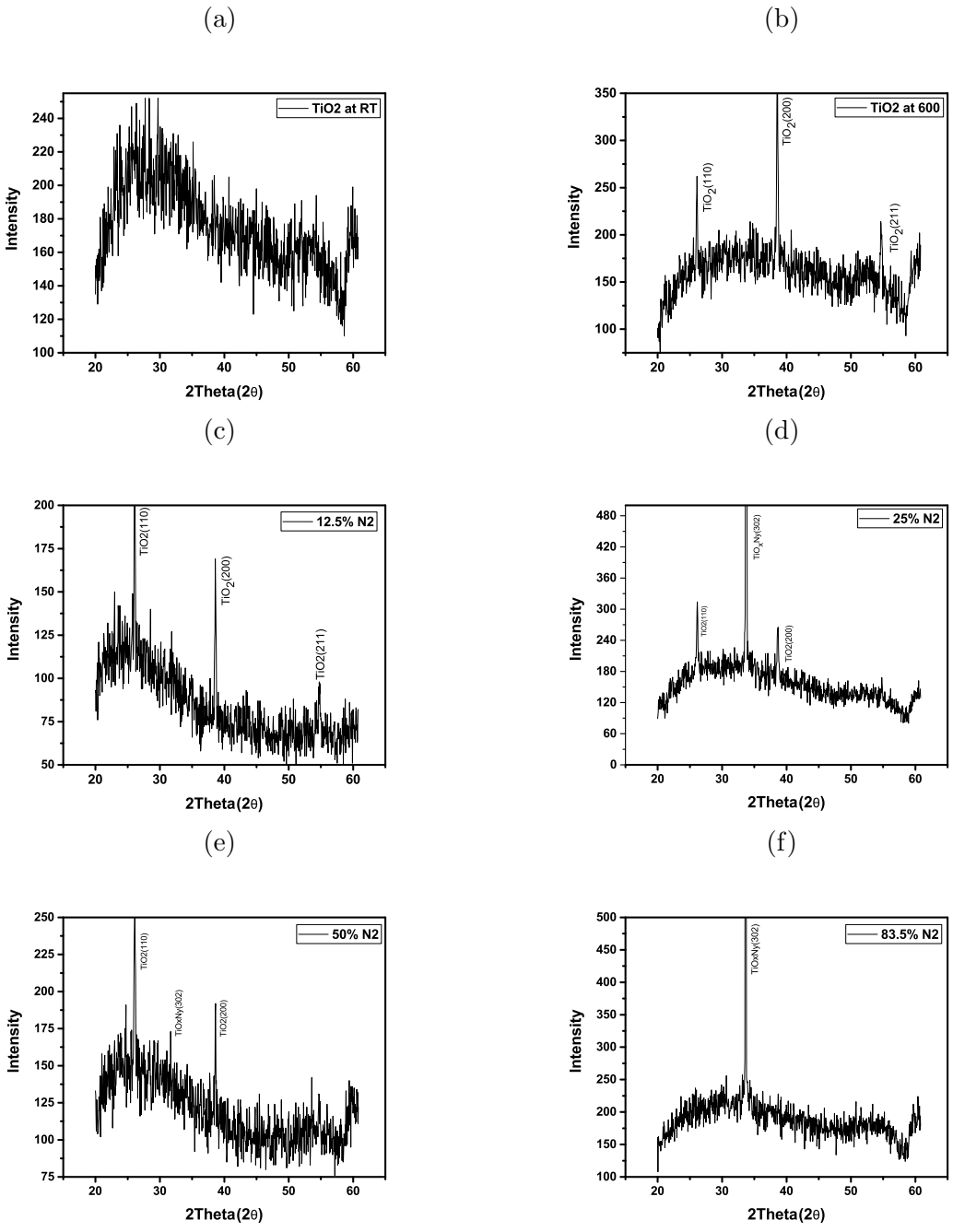

Figure 5.13: XRD Graphs of (a) Undoped TiO_2, 12.5% N doped TiO_2 , 25% N doped TiO_2, 50% N doped TiO_2 and 83.5% N doped TiO_2

5.2.2 SEM

Figure 5.14 shows the Field Emission Scanning Electron Microscope micrographs of fabricated TiO_2 and $TiO_{2-x}N_y$ thin films. Surface morphology contains the important information regarding size, shape, orientation, porosity, and distribution of particles or grains in thin films.

Surface morphology of TiO_2 thin films grown at room temperature is shown in figure 5.14(a). It have no specific grain direction or shape which reveals that no specific grain growth occurs at this temperature. Further XRD result of thin films confirms the amorphous nature of the thin films. Figure 5.14(b) shows surface morphology of TiO_2 annealed at 600° which shows very little grains that are evenly distributed over the whole surface. There is no specific shape of the grain, these are randomly oriented and is of nanometer (nm) size. Figure 5.14(c) shows the morphology of 12.5% Nitrogen(N_2) doped TiO_2 annealed at 600°. It can be seen that now the concentration of N_2 is doped in lattice of TiO_2 , the size of the grain increases from nano meter (nm) to micro meter (μm). The length of the grain size is varied in different microns. All of the grains are almost evenly distributed such that the lengths are almost equal of all grains and these are separated by grain boundaries. Figure 5.14(d) shows the morphology of 25% Nitrogen(N_2) doped TiO_2 annealed at 600°. It can be seen that now the concentration of N_2 is increased from 12.5% to 25% and is doped in lattice of TiO_2 , the size of the grain increases in micro meter (μm) regime. Figure 5.14(e) depicts the morphology of 50% Nitrogen(N_2) doped TiO_2 annealed at 600°. It can be clearly seen that as soon as concentration of N_2 is increased in lattice of TiO_2 , the size of the grain increases from nano meter (nm) to micro meter (μ) m. All of the grains are almost evenly distributed such that the lengths are almost equal of all grains and these are separated by grain boundaries. Fig 5.14(f) depicts the morphology

of 83.5% Nitrogen(N_2) doped TiO_2. This lattice is at room temperature, so no grains or grain boundaries are formed and very small sized particles are observed with sharp crystallinity as confirmed by XRD analysis as well.

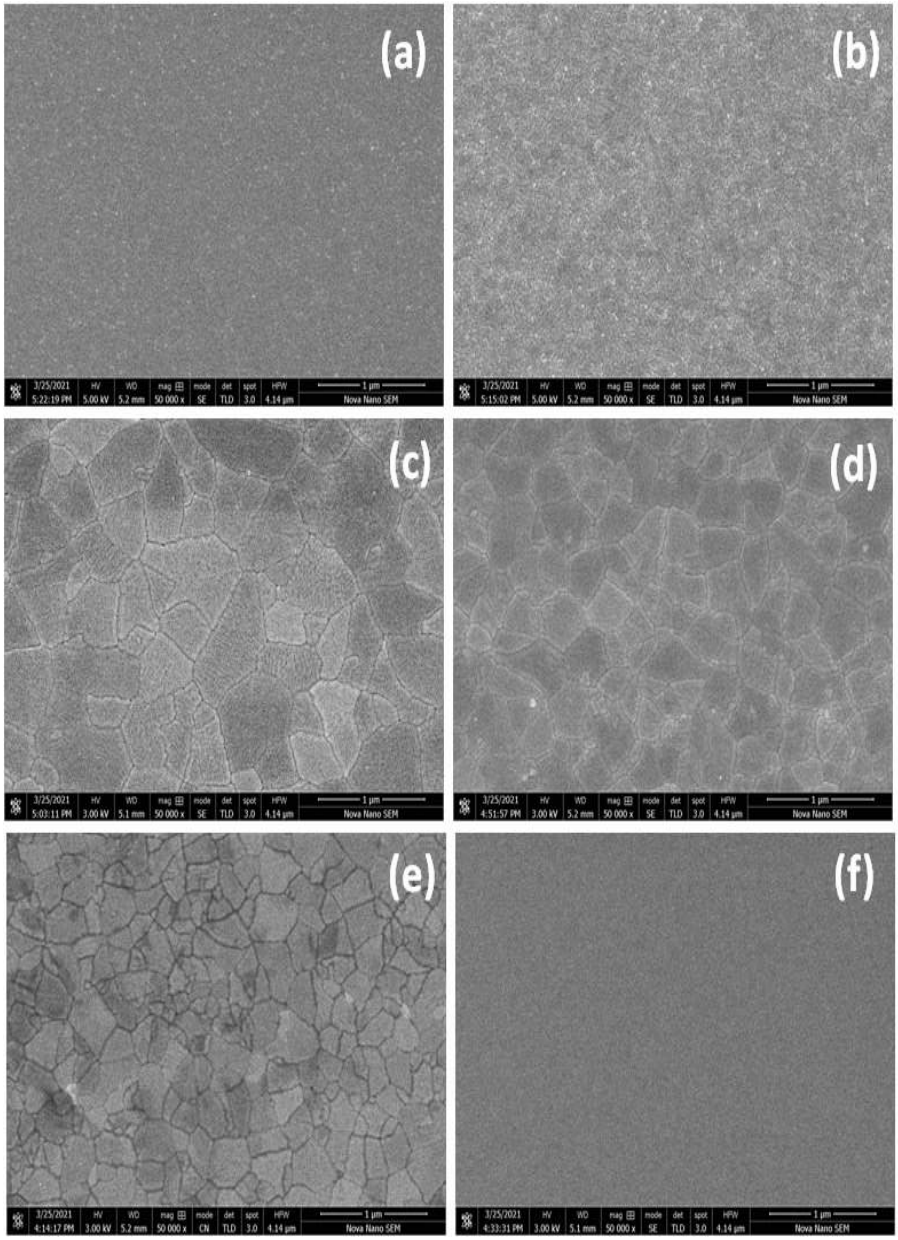

Figure 5.14: SEM of undoped TiO_2, 12.5% N2 doped, 25% N2 doped ,50% doped N2 and 83.4% doped N2 TiO_2

5.2.3 EDX

Elemental composition analysis of TiO_2 and N doped TiO_2 thin films shows that all elements with their respective stiochiometry ratio are existing in each corresponding structure as shown in figure 5.15. The elemental peaks coming in the pattern are assuring the presence of Ti, O and N material, Moreover there are also some other peaks that are telling about the presence of substrate. The elements with their corresponding percentages and weights are obtained from this energy dispersive x-ray analysis. These are the thin films therefore the peak of the substrate that is Si is very high in the pattern.

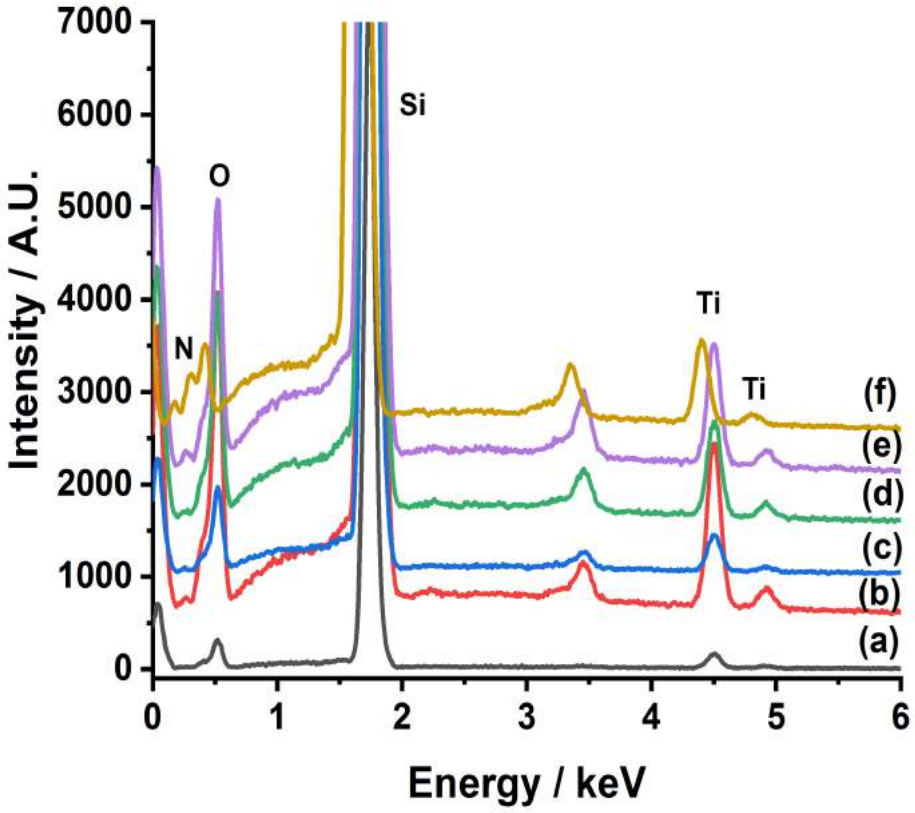

Figure 5.15: EdX of undoped TiO_2, 12.5% N2 doped, 25% N2 doped ,50% doped N2 and 83.4% doped N2 TiO_2

5.2.4 Raman Shift

Rutile phase of TiO_2 have been observed in the pure and N doped TiO_2 thin film samples by Raman spectroscopy. It belongs to the tetragonal system. Rutile phase belongs to the symmetry group with two formula units per unit cell. In case of raman modes oxygen atom forms vacancies. It is Excited with 532 nm laser light, while these emissions are absent in illuminating bulk TiO_2.

The spectrum acquired with 532 nm excitation is typical of those reported in the literature; it consists primarily of the E12g band at 383 cm^{-1} and the A1g band at 600 cm^{-1} as shown in the figure 5.16 as well as the Si substrate Raman band at 520 cm^{-1}.

Figure 5.16 shows the raman spectra of N doped TiO_2 thin films. The increment of N content creates a substantial change in the vibration modes. The peak intensity attenuation generally shows an enhancement in the structure disordering. In the 83.5% N doped TiO_2 film, the main peaks observed are related to the rutile structure around 500 cm^{-1}. This characteristic raman line of rutile phase observed at 510 cm^{-1} has a reported tenfold greater intensity than any other phonons for this phase. Higher contribution of rutile phase has been observed in higher concentration N doped samples as shown in XRD section.

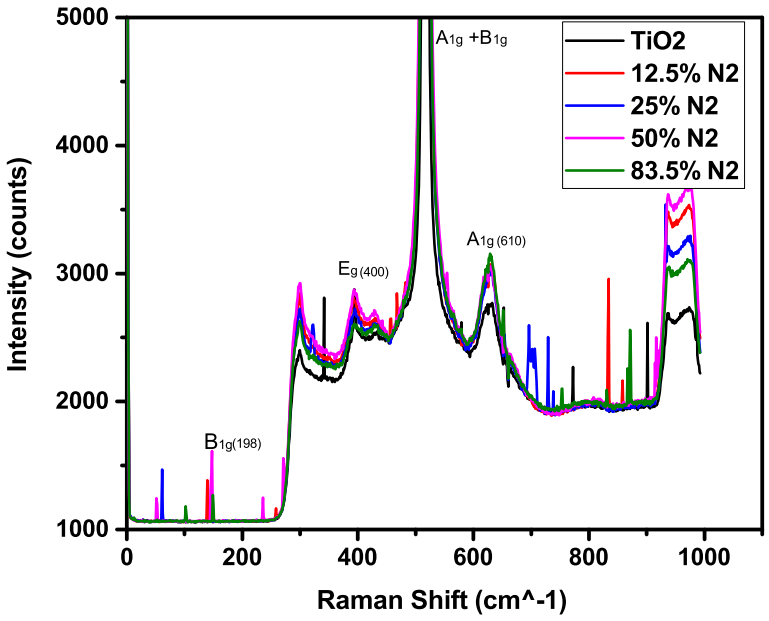

Figure 5.16: Raman Spectra of undoped TiO_2, 12.5% N2 doped, 25% N2 doped ,50% doped N2 and 83.4% doped N2 TiO_2

In figure, a gradual decrease in the intensity peaks of the Eg mode is observed as the N content increases and also shifted towards lower frequencies. Increase in rutile phase is in good agreement with the XRD results. Also we can say that as N atom mass is heavier than Ti atom, so we get peak shifting toward lower frequency with heavier N incorporation in the TiO_2 lattice.

5.2.5 Photolumniscence (PL)

The light emission spectra of the pure and N doped TiO_2 thin films with excitation wavelength of 325 nm is shown in the figure. In all the samples, emission band intensity approaches gradually towards maximum and then towards the zero minimum with the photonic energy.

In figure 5.17, for undoped TiO_2, the peak around 1.8 is observed. PL peak

spectrum observed arises due to the self exciton–photon interactions inside the material TiO_2. With the increasing nitrogen concentration, the PL spectrum peak intensity decreases and it is assumed that the doped N^{+3} ions have capture photo-generated holes, hence they suppresses the recombination and also PL intensity. The more the greater the concentration of N^{+3} ions, weaker would be PL intensity. As the charge state for the dopant and host Ti are not same, so doping with the N ions generally causes the formation of oxygen vacancies to sustain charge impartiality.

In case of 12.5% N doping as shown in the figure 5.17, we observed the peak splitting of undoped TiO_2 into multiple peaks. In this way as concentration of Nitrogen increases, the peaks splits at different values of energies(eV). Besides, in case of 83.5% doped N , maximum peak intensity is observed.

Generally, the photoluminescence excited at 532 nm is substantially weaker rel-

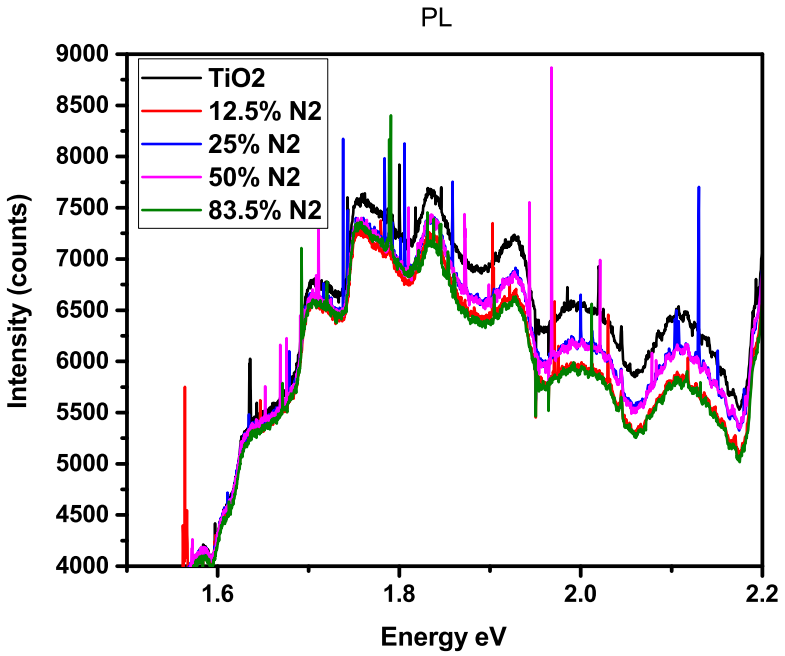

Figure 5.17: PL of undoped TiO_2, 12.5% N2 doped, 25% N2 doped ,50% doped N2 and 83.4% doped N2 TiO_2

ative to the Raman scattering when compared to the photoluminescence-Raman strength ratio of the 632.8 nm excited spectrum. An important aspect of this measurement is that one can simultaneously obtain a Raman spectrum and a photoluminescence spectrum from the same location. That fact holds important implications for the ability to simultaneously perform photoluminescence and Raman imaging of few-layer TiO_2.

Chapter 6

Conclusion

Ab-initio calculations were performed for electronic and optical response of pure rutile Titania and Titanium oxynitride thin films using Wien2k code by varying the nitrogen content in structure. DOS spectra reveal p-orbital of oxygen atom and d-orbital of Ti atom contributes to produce p-d hybridization in TiO_2 structure while additional contribution from nitrogen atom in Titanium oxynitride structures. Band structure reduced with the increment of nitrogen concentration and overlapping at fermi level observed in these compositions attributed to an enhanced n-type conductivity. Optical properties like absorption coefficient, reflectivity, extinction, refractive index and epsilon were varied with nitrogen content. Simulation results predicts ENZ response in titanium oxynitride structures. Thin films of pure rutile titania and titanium oxinitride with variation of nitrogen and oxygen ratio were deposited on silicon substrate for experimental investigations. XRD spectra of thin films show an amorphous and rutile structure of titania thin films produced at room temperature and 600 ∘C, respectively. Crystallinity of thin films undergoes a steady change with incorporation on nitrogen content as observed from the peak positions, and intensity. A sharp change in crystalline phase was observed in thin film composition having highest content

of nitrogen. Morphology and elemental composition of thin films confirms the structural findings and phase purity. Morphology shows randomly distributed grains of different sizes having sharp grain boundaries in titanium oxinitride thin films while EDX analysis confirms the presence of expected elemental contents in respective thin films. The composite phases of TiO_2, TiN, and TiO_xNy were observed during experimental observations. Optical properties have minute contradiction with theoretical calculations due to presence of these phases. The absorption coefficient found to increase with the increase of nitrogen content in structure attributed to the perfect absorption of these type of thin films. ENZ response however successfully achieved in thin films having highest content of nitrogen exactly following the simulation curve.

Bibliography

[1] Joy George. *Preparation of thin films*. CRC Press, 1992.

[2] Ulrike Diebold. The surface science of titanium dioxide. *Surface science reports*, 48(5-8):53–229, 2003.

[3] S Tripura Sundari, R Ramaseshan, Feby Jose, S Dash, and AK Tyagi. Investigation of temperature dependent dielectric constant of a sputtered tin thin film by spectroscopic ellipsometry. *Journal of Applied Physics*, 115(3):033516, 2014.

[4] Mel Levy. Universal variational functionals of electron densities, first-order density matrices, and natural spin-orbitals and solution of the v-representability problem. *Proceedings of the National Academy of Sciences*, 76(12):6062–6065, 1979.

[5] David J Thouless. Stability conditions and nuclear rotations in the hartree-fock theory. *Nuclear Physics*, 21:225–232, 1960.

[6] Lars Hedin and Bengt I Lundqvist. Explicit local exchange-correlation potentials. *Journal of Physics C: Solid state physics*, 4(14):2064, 1971.

[7] Peter MW Gill. Density functional theory (dft), hartree-fock (hf), and the self-consistent field. *J. Chem. Phys*, 100:5066–5075, 1994.

[8] Miguel AL Marques, Micael JT Oliveira, and Tobias Burnus. Libxc: A library of exchange and correlation functionals for density functional theory. *Computer physics communications*, 183(10):2272–2281, 2012.

[9] V Ozoliņš and M Körling. Full-potential calculations using the generalized gradient approximation: Structural properties of transition metals. *Physical Review B*, 48(24):18304, 1993.

[10] P Blaha et al. Linear methods in band theory. *Phys. Rev. B Solid State*, 12:3060, 1975.

[11] E Sjfistedt, L NordstrOm, and DJ Singh. An alternative way of linearizing the augmented plane-wave method [jt. *Solid State Comm*, 114:15–20, 2000.

[12] Karlheinz Schwarz. Dft calculations of solids with lapw and wien2k. *Journal of Solid State Chemistry*, 176(2):319–328, 2003.

[13] Sophocles J Orfanidis. Electromagnetic waves and antennas. 2002.

[14] John Weiner and Frederico Nunes. *Light-matter interaction: physics and engineering at the nanoscale*. Oxford University Press, 2017.

[15] Marc J Madou. *Fundamentals of microfabrication: the science of miniaturization*. CRC press, 2018.

[16] Kaifeng Shi and Zhaolin Lu. Field-effect optical modulation based on epsilon-near-zero conductive oxide. *Optics Communications*, 370:22–28, 2016.

[17] Xin Li. *Epsilon-near-zero metamaterials for optoelectronic applications*. PhD thesis, University of St Andrews, 2019.

[18] Md Alamgir Badsha, Young Chul Jun, and Chang Kwon Hwangbo. Admittance matching analysis of perfect absorption in unpatterned thin films. *Optics Communications*, 332:206–213, 2014.

[19] Peter J Kelly and R Derek Arnell. Magnetron sputtering: a review of recent developments and applications. *Vacuum*, 56(3):159–172, 2000.

[20] Charles Kittel, Paul McEuen, and Paul McEuen. *Introduction to solid state physics*, volume 8. Wiley New York, 1996.

[21] Michael Eckert. Max von laue and the discovery of x-ray diffraction in 1912, 2012.

[22] Bc Ján Bella. Imaging distortion correction in panorama stitching in sem. *Masaryk University*, 2017.

[23] Hani F Ounsi, Thakib Al-Shalan, Ziad Salameh, Simone Grandini, and Marco Ferrari. Quantitative and qualitative elemental analysis of different nickel–titanium rotary instruments by using scanning electron microscopy and energy dispersive spectroscopy. *Journal of Endodontics*, 34(1):53–55, 2008.

[24] Bob Hafner. Energy dispersive spectroscopy on the sem. *Characterization Facility, University of Minnesota, USA*, 2011.

[25] VA Solé, E Papillon, M Cotte, Ph Walter, and JA Susini. A multiplatform code for the analysis of energy-dispersive x-ray fluorescence spectra. *Spectrochimica Acta Part B: Atomic Spectroscopy*, 62(1):63–68, 2007.

[26] Australian Microscopy. Microanalysis research facility. *Scanning Electron Microscope Training module*, 2014.

[27] R Amraoui, M Doghmane, S Chettibi, and DF Laefer. The electronic structure and optical properties of rutile tio2 co-doped with nickel and cerium. *Chinese journal of physics*, 55(6):2393–2399, 2017.

[28] Sajad Hussain, Chuanbao Cao, Ghulam Nabi, Waheed S Khan, Muhammad Tahir, Muhammad Tanveer, and Imran Aslam. Optical and electrical characterization of zno/cuo heterojunction solar cells. *Optik*, 130:372–377, 2017.

[29] Frederick Wooten. Optical properties of solids. *American Journal of Physics*, 41(7):939–940, 1973.

[30] Edward D Palik. *Handbook of optical constants of solids*, volume 3. Academic press, 1998.

[31] Stephen K O'Leary, SR Johnson, and PK Lim. The relationship between the distribution of electronic states and the optical absorption spectrum of an amorphous semiconductor: An empirical analysis. *Journal of applied physics*, 82(7):3334–3340, 1997.

[32] P Carvalho, F Vaz, L Rebouta, L Cunha, CJ Tavares, C Moura, E Alves, A Cavaleiro, Ph Goudeau, E Le Bourhis, et al. Structural, electrical, optical, and mechanical characterizations of decorative zr o x n y thin films. *Journal of applied physics*, 98(2):023715, 2005.

[33] Jesús Graciani, Said Hamad, and Javier Fdez Sanz. Changing the physical and chemical properties of titanium oxynitrides tin 1- x o x by changing the composition. *Physical Review B*, 80(18):184112, 2009.